# Supplemental online material for "Microstructural changes and Pb mobility during the zircon to reidite transformation: implications for planetary impact chronology" by Szumila et al.

## Methodology

### Details on methods

Here further information is presented on the methods aspects of both the pre- and post-shock material discussed in the main text. The parameters used for each analytical instrument and analytical session are detailed. Further information on how experimental simulations using iSALE2D were set up is presented.

### iSALE2D simulation parameter selection

Since the target material is mostly sanidine, all material in the target well was modeled as sanidine, ignoring the zircon component since zircon only comprised 3 wt% of the mix. The sample container and flyer plate were modeled as 304 stainless steel using the Mie-Grüneisen EoS parameters from Gleason et al., (2020) with 304 stainless steel heat capacity (Bogaard et al., 1993; Bentz and Prasad 2007) calculated at 25 °C (298 K). Another custom Mie-Grüneisen equation of state (EoS) was used to simulate the sanidine. The density of sanidine was set to 2.58 g/cm$^3$ (Wapels and Wapels, 2004), $3.10\times10^3$ m/s as the speed of sound inside sanidine feldspar (Ahrens and Johnson, 1994), the slope constant in the linear shock wave-particle velocity relationship was set to 1.39 (Ahrens and Johnson, 1994). As an estimate for the Grüneisen parameter, the value 0.42 from Tribaudino et al. (2011) was used; this value is for a plagioclase feldspar but was used as an

approximation for the simulation. This sets all parameters needed to the use the Mie-Grüneisen EoS in iSALE2D. The simulation used a heat capacity for high sanidine material calculated at 1000 ℃ (1273 K) and assumed constant at 1164 J/(kg sanidine × T[in K]) using the heat capacity equation from Hemingway et al., (1981). Hydrocode solvers simulate an incomplete EoS over the density and internal energy domains. During the simulation, a few steps are implemented that allow iSALE2D to calculate a temperature when using Mie-Grüneisen equations of state. First, the internal energy due to compression is calculated from a numerical integral. Then this value is subtracted from the total internal energy. This gives the internal energy due to thermal components only. This final value is divided by the heat capacity (assumed constant and non-temperature dependent) to approximate the temperature (see section 4.1.7 in Collins et al., 2016). The values used for these parameters and the source literature for the values are summarized (**Table S1**) and the input files for the simulation are available in the rest of the online repository as well.

**SEM Methods**

Unshocked starting material and shocked material from the flat-plate experiment were imaged via SEM and analyzed with Energy Dispersive X-Ray Spectroscopy (EDS). Before analysis the samples were coated with 40 nanometers of Au using an MCM-200 Ion Sputter Coater. Analyses were performed at the University of Alabama on a JEOL JSM-7000F using an accelerating voltage of 20 kV and a working distance of 10 mm. Some SEM images (e.g. **Figure 1c**, **Figure 3b**) were generated later via another analysis at the University of Rochester with a Hitachi TM4000Plus Tabletop Microscope. These analyses used the same working distance but an accelerating voltage of 15 kV. Samples were carbon coated before this second analysis.

**Raman spectroscopy methods**

Raman spectroscopy was done with a Reinshaw inVia Raman Microscope at NASA JSC. This instrument was used to collect spectra from both unshocked sanidine and unshocked zircon, as well as material subjected to the shock experiment. The wavelength of the laser was 633 nm with a LEICA 50x objective lens and diffraction grating of 1800 lines/mm. Exposure times were kept at 50 s. Raman shifts were measured between 100 $cm^{-1}$ to 2000 $cm^{-1}$. Additional spot Raman analyses, collected on all sample materials, was acquired during revisions using a Renishaw inVia Raman Microscope at Syracuse University. The wavelength of the laser for these analyses was 532 $cm^{-1}$ using a 50x LEICA objective, with a diffraction grating of 1800 lines/mm. Exposure times were 10s and the Raman shift was measured between 100 $cm^{-1}$ to 4200$cm^{-1}$ for every analysis. For Raman mapping, A WITec alpha300R Confocal Raman Microscope (again at NASA JSC) was rastered on an unshocked piece of the starting zircon used in the experiment. This instrument used a laser wavelength of 488 nm, a Zeiss 20x objective lens, and a grating with 300 l/mm. The spectral range of the collected spectra was 3600 $cm^{-1}$. The total size of the map raster was 3104×1752 μm, which corresponds to 388×219 Raman pixels at 8 $\mu m^2$. Integration per pixel was 0.5 s, with the total scan taking ~12 h. For the Raman map, the data collection and data processing was done with the WITec Suite FIVE software. The map was made using WITec's Basic Analysis feature which compares collected spectra to example spectra and assigns a fit score for each. For the Basis Image function used to make this map, the intensity of each pixel is the fit score with the multi-color overlay being produced via user-selected threshold values for the fits.

## Electron backscatter diffraction (EBSD) and transmission EBSD methods

Use of EBSD allows investigations into crystallographic orientation relationships and polymorphism by indexing phases based on the crystal structure. Select post-shock $ZrSiO_4$ material was analyzed by EBSD using the JEOL 7600f SEM at NASA JSC, with an accelerating voltage of 20 kV and a probe current of 9.5 nA. An Oxford Instruments Aztec Symmetry detector attached to the SEM was used to collect diffraction patterns. A second EBSD technique known as transmission Kikuchi diffraction (TKD) allows for high resolution (sub-10 nm) imaging of an electron-transparent sample foil. Liftout of the foil was done using an FEI Quanta focused ion beam (FIB) SEM at NASA JSC with a 30 kv Ga ion beam, and 0.30 nA probe current. The TKD analyses were performed with the same EBSD detector and SEM mentioned above. All EBSD and TKD data were post processed using the Channel5 program suites Tango and Mambo to produce maps and pole figures, respectively.

## LA-ICP-MS analytical methods

Laser Ablation-Inductively Coupled Plasma-Mass Spectrometry (LA-ICP-MS) was conducted at the University of Rochester (UR) and the University of Houston (UH). The UR LA-ICP-MS system was used to analyze the experimentally shocked sanidine. This system uses a Photon Machines 193 nm ArF laser coupled to an Agilent 7900 mass spectrometer. Parameters used at UR included a laser repetition pulse rate of 10 Hz, a circular spot size of 35 μm, a fluence of 6.75 J/cm$^2$, a shot count of 200 per spot. The carrier gas flow rates were set at 0.600 He l/min for Mass Flow Controller 1 (MFC1) and 0.200 He l/min for MFC2 (Trail et al., 2017). A session at UR in which unshocked sanidine was analyzed used the above parameters except for a higher

laser fluence of 10.72 J/cm$^2$. The UH has a Photon Machines Excite 193 nm ArF laser coupled to a Varian 810 ICP-MS, which were used to analyze unshocked zircon and post-shock reidite material. Parameters at UH were a laser repetition rate of 10 Hz, spot size of 35 μm circle, and fluence of 3.74 J/cm$^2$ and a shot count of 300 per spot. At UH, gas flow rates used for the sample cell were 0.420 He l/min for MFC1 and 0.320 He l/min for MFC2 in order to get the best signal from the sample cell. Instrumental mass and element fractionation were corrected using methods outlined in Shaulis et al. (2010; 2017). Some LA-ICP-MS data was also processed with Iolite V3.61 in the Igor Pro environment, using the X_U_Pb_Geochron4 data reduction scheme. Individual LA-ICP-MS analyses for the reidite, unshocked zircon and $ZrSiO_4$ material are presented in **Table S3**.

**SIMS analytical methods**

The SIMS U-Pb dating on unshocked zircon and shocked reidite was done using the CAMECA *ims*1290 ion microprobe at UCLA with Hyperion-II RF oxygen plasma source (Liu et al., 2018). The analytical procedure was similar to that reported for the *ims*1290 by Sequeira et al. (2021). A ca. 3 nA $O_3^-$ primary beam was focused to a ca. 6 μm spot and accelerated with a − 13 kV primary voltage to a stage held at ca. +10 kV. Analyses were run at a mass resolving power (MRP) ca. 5000. Masses collected include $^{180}Hf^{16}O^+$, $^{94}Zr_2{}^{16}O^+$, $^{204}Pb^+$, $^{206}Pb^+$,$^{207}Pb^+$,$^{208}Pb^+$, $^{232}Th^+$, $^{238}U^+$, $^{238}U^{16}O^+$, and $^{238}U^{16}O_2{}^+$. Pb/U RSF was determined for unknowns using the correlation of $UO_2$/U vs $^{206}Pb/^{238}U$ RSF for the AS3 zircon standard (e.g., Schmitz et al., 2003). Analyses of the 91500 zircon standard were used as a secondary check for age accuracy and to determine the RSF for $HfO/Zr_2O$, $Th/Zr_2O$, and $U/Zr_2O$ using the concentrations reported by Wiedenbeck et al. (2004).

For reidite and unshocked non-metatmict zircon, 10 spots were analyzed each. For the unshocked but metamict $ZrSiO_4$ spots, 7 spots were analyzed with SIMS. Out of these 7, 1 spot was rejected due to an anomalously high $^{238}UO_2/^{238}U$ suggesting that for at least part of that analysis the beam may have encountered another phase. This resulted in the 6 analyses averaged for the metamict $ZrSiO_4$ average presented in Table 1 for $ZrSiO_4$. All individual SIMS analyses for the reidite, intact zircon, and metamict $ZrSiO_4$, are presented in **Table S4** while individual SIMS analyses for sanidine are present in **Table S5**.

In order to better estimate the common Pb contamination on shocked sample, additional Pb isotopic analyses of the shocked sanidine with similar MRP and an 8 nA primary beam were performed. Masses measured included $^{204}Pb^+$, $^{206}Pb^+$,$^{207}Pb^+$, and $^{208}Pb^+$. Several analyses of NIST-610 standard glass were also undertaken under these same conditions to establish the lack of instrumental mass fractionation among Pb isotopes. For standard zircons and the unshocked unknown zircon, common Pb was assumed to derive from laboratory contamination and was estimated from $^{204}Pb$ abundance using the isotopic ratios of San Diego Sewage (Sañudo-Wilhelmy and Flegal, 1994). For the shocked reidite, $^{204}Pb$ corrections were also done but assuming common Pb contamination would derive from the shocked sanidine.

## Additional supporting results

### Additional iSALE2d results and experiment P-T modeling

Using the tracer feature of the iSALE2d software, we can track the average pressure of all tracers in the simulation for each timestep. Therefore, a plot of average pressure vs time, average

temperature vs. time and average pressure for average temperature are show **Figure S1**. The max average pressure at a single timestep is close to ~25 GPa (**Figure S1A)**. This matches with the expected result from impedance matching a stainless steel flyer plate into a stainless steel target at 1.132 km/s, thus demonstrating that the iSALE2D hydrocode matches predicted values. The temperature vs time plot shows a rapidly increasing temperature during the shock event followed by the average temperature dwelling at ~1100 K (**Figure S1B**). When average pressure and average temperature are plotted together (**Figure S1C**), it can be seen that the entire pressure spike from the experiment occurs within the timeframe of the simulation while the thermal effects linger longer. These averages show that a number of tracers reached higher pressure and temperatures as well, so a broader range of P-T conditions were likely experienced by the sample.

Additional data from the simulation in the main text are featured in the next set of figures. A re-plot of **Figure 9a** from the text with temperature instead of pressure is shown (**Figure S2**). Animations of the impact simulation are shown in **Figure S3** and **Figure S4.** An animation showing the evolution of the pressure and temperature for all tracers as the simulated experiment proceeds is also shown (**Figure S5**).

**SEM analyses and high U-Th regions**

A re-plot of SEM analysis of Figure 1 in the main text with additional labeling is shown (**Figure S6**) to offer more insight on the grains analyzed. The SEM analyses of a portion of an unshocked zircon fragment sourced from the same rock as that used in the shock experiment are pictured (**Figure S7**) along with as unshocked sanidine. The image confirms that the sanidine is

clean and featureless. For the zircon, these analyses indicate that while the primary material is zircon, the zircons from this rock have inclusions, notably the U-Th oxides discussed in the text. These backscatter bright regions were identified in shocked material as well where EDS analysis showed them to be areas of high U-Th contents (**Figure S8**). These U-Th phases likely contributed to the metamictization of the starting material.

**Zirconia beads**

A box around a particular backscatter-bright region for grain A in the lower left corner (**Figure S9**) shows an area of interest. Close-ups views of this region are provided (**Figure S10a**). This region is mostly $ZrSiO_4$. However, tiny (<0.3 μm) beads of some other material can be seen, which were only observed in the shocked materials (**Figure S10b)**. The beads observed here in the shocked materials are not the same feature as the U-Th phases that were identified in both shocked and unshocked material and discussed in the text. These beads were analyzed by EDS (**Figure S10d**), although it is difficult to produce an interaction volume small enough to yield X-rays only from these beads and exclude secondary fluorescence effects from the surrounding phases. Therefore, the EDS spectra from these regions contain some contribution from the surrounding wispy regions as well. Although this is qualitative, the collected EDS spectra seem to indicate slightly higher Zr and less Si wt% than would be expected from zircon alone, or one of its higher-pressure polymorphs. We hypothesize these tiny (<0.3 μm) beads embedded in a wispy backscatter bright region of amorphous $ZrSiO_4$ could be small nucleated zirconia produced during the shock experiment. This has implications for the *P-T* conditions achieved in these regions. If these are a $ZrO_2$ polymorph (e.g., baddeleyite), then the temperature for decomposition of either zircon or reidite to $ZrO_2$ and $SiO_2$ should have been reached at least locally. At 22 GPa and 1000 °C (1273

K), reidite will transition to $SiO_2$ and $ZrO_2$ phases (Liu, 1979; Chen et al., 2013). At ambient pressure, zircon will decompose to $SiO_2$ and tetragonal $ZrO_2$ at 1673 ℃ (1946 K) (Timms et al., 2017a).

**Sanidine major wt% element LA-ICP-MS analyses**

In order to analyze structural damage in the sanidine, its major wt% components (e.g. Al and K) were also characterized via LA-ICP-MS. The shocked and unshocked sanidine exhibit only a small difference in major element compositions and all are that within 2 s.e. of each other (**Table S2)**. Specifically, two unshocked sanidines yield Al and K weight % content of 10.84 ± 0.34 (2 s.e.) and 9.72 ± 0.29 respectively, whereas the shocked sanidine yields Al and K weight % content 10.78 ± 0.19 and 9.62 ± 0.15. An average of 8 LA-ICP-MS spots on the shocked sanidine material has Al and K weight % 10.05 ± 0.22 and 10.29 ± 0.23 respectively.

**Raman map reprocessing**

There are a number of fractures cutting across a large portion of the unshocked grain material (**Figure 3a** in the text). The fractures in the grain probably formed through structural expansion (Nasdala et al., 2002) from metamictization of the grain. The same Raman spectral map data that was present in the text (**Figure 4b**) was re-processed in a separate way as well (**Figure S11**) where red identifies zircon regions, green designates carbonate regions, and blue is used for possible uranophane regions. When done, the fractures coincide with blue lines (**Figure S11)**. We consider this evidence that the grain experienced groundwater alteration that utilized the existing fracture network caused by expansion of the crystal lattice during metamictization. Since the blue

lines permeating these fractures were identified as an uranophane phase, there is a strong possibility that a groundwater alteration event deposited the U-Th oxide phases found in the grain and explains their presence.

Grain B was referred to as $ZrSiO_4$ material that has been fully amorphized in the main text. A number of Raman spectra analyzed on grain B along with Raman spectra from partially and fully metamict regions on the starting grain are presented for comparison (**Figure S12)**. This data shows that in broad terms, grain B mostly lacks crystalline structure.

**LA-ICP-MS concordia results**

The LA-ICP-MS analyses of the unshocked zircon and the post-shock reidite were plotted together in **Figure S14** to make a concordia diagram using only the U-Pb results as analyzed by LA-ICP-MS. Only one LA-ICP-MS spot was placed on the reidite to conserve as much of the grain as possible for the SIMS analyses. The results (**Figure S14**) suggested that it was not possible to detect mobilization of Pb between the unshocked zircon and the reidite within the precision of LA-ICP-MS. This agrees with the result of the main text that shock alone is not responsible for disturbance of the U-Pb ages in zircon and reidite. The LA-ICP-MS analysis data is presented in **Table S2** which shows the analyses for the single spot on the reidite, the 16 spots comprising the vertical traverse, and 6 additional spots making up a horizontal traverse.

**Additional EBSD analyses**

Other grains were also analyzed by EBSD and these results are displayed (**Figure S15**, **Figure S16**, and **Figure S17**). The results are congruous with those of the main text. Reidite and zircon can be identified in these images although in many cases with reidite domains of up to 50 μm across. The {112} twins in reidite (Leroux et al., 1999) can also be seen in the material that indexed as reidite in these images.

**Reidite Th/U, MSWD analyses, Dα radiation damage and additional discussion of the SIMS data**

The Th/U of the SIMS analyzed spots on the reidite have been plotted along with their $^{207}Pb/^{206}Pb$ ages (**Figure S18**) which helps to assuage concern over heterogeneity in the starting material that produced the reidite. Since there are not any large Th/U variations in the spots around the reidite grain, it is very unlikely that any of the high Th/U material discussed in section 2.2 interfered with the geochronology case being made about the reidite. Next, comparisons of the MSWD of the zircon and reiditie ages (**Figure S19**) also provide insight and inform that the $^{207}Pb/^{235}U$ age is the U-Pb age system least disturbed by the impact loading process. The MSWD values when calculated for the SIMS $^{207}Pb/^{206}Pb$, $^{207}Pb/^{235}U$ and $^{206}Pb/^{238}U$ ages in the unshocked and non-metamict zircon are all less than 1. When the MSWD is calculated for each of these values for reidite, the MSWD is greater than 1 for the $^{207}Pb/^{206}Pb$ and $^{206}Pb/^{238}U$ ages but <1 for the $^{207}Pb/^{235}U$. This indicates there is still a large amount of scatter in the reidite ages but that the $^{207}Pb/^{235}U$ age may be more reliable than the other geochronometers. It also appears that the zircon to reidite transition could be related to increased MSWD seen for the reidite ages. So although age

in the reidite was not reset by the shock experiment, increased scatter in the post-shock reidite ages may have resulted in a higher MSWD.

When characterizing the starting material, we primarily relied on the Raman map to determine if a region was intact zircon, partially metamict or fully metamict $ZrSiO_4$. However radiation damage in the zircon can also be understood if the age of the grain and current U-Th concentrations are known. This is achieved by calculating the number of alpha-decay events per mg the grain would have experienced (Palenik et al., 2003) based on the U and Th decay chains. This information can then additionally be used to calculate displacements per atom (dpa) although this is generally an overestimate since it does not account for thermal annealing which would heal the crystal structure. Murakami et al., 1991 separates out radiation damage to three stages based on TEM analyses, with Stage I (alpha-decay events/mg$<3\times10^{15}$), Stage II ($3\times10^{15}<$alpha-decay events/mg$<8\times10^{15}$) and Stage III (alpha-decay events/mg$>8\times10^{15}$). The SIMS analyses on our intact zircon material (that is the material identified as the blue region in **Figure 3a & c**) generally have calculated (using the $^{206}Pb/^{207}Pb$) $D_\alpha$ values between approximately $2\times10^{15}$ and $5\times10^{15}$. This shows that most of the starting zircon has moderate metamictization. These values were also calculated for the reidite SIMS analyses as well as the SIMS analyses on the fully metamict region in the saved portion of the starting zircon. The spots on reidite because of the lower U-Th values generally shows lower $D_\alpha$ with only two spots (out of 10) having a calculated Dα just above $3\times10^{15}$ and none greater than $3.4\times10^{15}$. It is not known if this lower U and Th in reidite is from the shock experiment or simply because this reidite is derived from a portion of the starting material with a varying amount of U or Th from the rest of the grain. As expected the fully metamict region, due to its extremely high U and Th contents, consistently has calculated $D_\alpha > 5\times10^{16}$ for all analyses.

Finally, the reader may wonder why the probability of concordance for the unshocked and non-metamict zircon is less than that of post-shock reidite in **Figure 7** from the main text. This is because the numbers reported in Figure 7 are the probabilities of concordance, but IsoPlot reports three values related to this which are the probability of equivalence, the probability of concordance and combined probability of equivalence and concordance. In cases where the U-Pb ellipses overlap both the concordia and each other, the probability of equivalence may also need be taken into account (e.g. Ludwig, 1998). Many of the analyses here for the intact zircon are similar enough, that the probability of concordance is actually lower than for the case of the reidite yet the probability of x-y equivalence for the intact zircon is 0.96 and the combined concordance and equivalence probability is 0.94. For the reidite, the probability of x-y equivalence is 0.013 and combined probability of x-y equivalence and concordance is 0.019.

## References (Supplemental)

Ahrens, T. J., and Johnson, M. L. (1994). Shock Wave Data for Minerals. NASA-CR-199490, 1–51.

Bentz, D.P., and Prasad, K. (2007) Thermal Performance of Fire Resistive Materials I. Characterization with Respect to Thermal Performance Models. U.S. Department of Commerce, NISTIR 7401, 1-21

Bogaard, R.H., Desai, P. D., Li, H. H. and Ho, C. Y. (1993) Thermophysical properties of stainless steels. Thermochimica Acta, 218, 373-393

Chen, M., Yin, F., Li, X., Xie, X., Xiao, W., and Tan, D. (2013). Natural occurrence of reidite in the Xiuyan crater of China. Meteoritics and Planetary Science, 48(5), 796–805.

Collins, G. S., Elbeshausen, D., Wünnemann, K., Davison, T. M., Ivanov, B., and Melosh, H. J. (2016). iSALE: A multi-material, multi-rheology shock physics code for simulating impact phenomena in two and three dimensions. ISALE-Dellen Release.

Dutta, R., and Mandal, N. (2012). Structure, elasticity and stability of reidite (ZrSiO4) under hydrostatic pressure: A density functional study. Materials Chemistry and Physics, 135(2-3), 322–329.

Hemingway, B. S., Krupka, K. M., and Robie, R. A. (1981). Heat capacities of the alkali feldspars between 350 and 1000 K from differential scanning calorimetry, the thermodynamic functions of the alkali feldspars from 298.15 to 1400 K and the reaction quartz * jadeite = analbite. American Mineralogist, 66, 1202–1215.

Liu, L.-G. (1979). High-pressure phase transformations in baddeleyite and zircon, with geophysical implications. Earth and Planetary Science Letters, 44(3), 390–396

Liu, M. C., McKeegan, K. D., Harrison, T. M., Jarzebinski, G., & Vltava, L. (2018). The Hyperion-II radio-frequency oxygen ion source on the UCLA ims1290 ion microprobe: Beam characterization and applications in geochemistry and cosmochemistry. International Journal of Mass Spectrometry, 424, 1-9.

Ludwig, K.R., (1998) On the treatment of concordant uranium-lead ages. Geochimica et Cosmochimica Acta, 62(4), 665–676.

Nasdala, L., Irmer, G., and Jonckheere, R. (2002) Radiation damage ages: Practical concept or impractical vision? – Reply to two comments on ‘‘Metamictisation of natural zircon: Accumulation versus thermal annealing of radioactivity-induced damage’’, and further discussion. Contributions to Mineralogy and Petrology, 143: 758–765

Palenik, C.S., Nasdala, L., Ewing R.C., (2003) Radiation damage in zircon. American Mineralogist, Volume 88, pg. 770–781

Quidelleur, X., Grove, M., Lovera, O. M., Harrison, T. M., Yin, A., & Ryerson, F. J. (1997). Thermal evolution and slip history of the Renbu Zedong Thrust, southeastern Tibet. Journal of Geophysical Research: Solid Earth, 102(B2), 2659-2679.

Sañudo-Wilhelmy, S. A., & Flegal, A. R. (1994). Temporal variations in lead concentrations and isotopic composition in the Southern California Bight. Geochimica et Cosmochimica Acta, 58(15), 3315-3320.

Schmitz, M. D., Bowring, S. A., & Ireland, T. R. (2003). Evaluation of Duluth Complex anorthositic series (AS3) zircon as a U-Pb geochronological standard: New high-precision isotope dilution thermal ionization mass spectrometry results. Geochimica et Cosmochimica Acta, 67(19), 3665-3672.

Sequeira, N., Bhattacharya, A., & Bell, E. (2021). The~ 1.4 Ga A-type granitoids in the “Chottanagpur crustal block”(India), and its relocation from Columbia to Rodinia?. Geoscience Frontiers, 101138.

Timms, N.E., Erickson, T. M., Pearce, M.A., Cavosie, A.J., Schmieder, M., Tohver, E., Reddy, S.M., Zanetti, M.R., Nemchin, A.A., and Wittmann, A. (2017a) A pressure-temperature phase diagram for zircon at extreme conditions. Earth-Science Reviews 165, 185-202.

Trail, D., Tailby, N., Wang, Y., Harrison, T. M., and Boehnke, P. (2017). Aluminum in zircon as evidence for peraluminous and metaluminous melts from the Hadean to present. Geochemistry, Geophysics, Geosystems, 18(4), 1580–1593.

Tribaudino, M., Bruno, M., Nestola, F., Pasqual, D., and Angel, R. J. (2011). Thermoelastic and thermodynamic properties of plagioclase feldspars from thermal expansion measurements. American Mineralogist, 96(7), 992–1002.

Shaulis, B., Lapen, T.J., and Toms, A. (2010) Signal linearity of an extended range pulse counting detector: Applications to accurate and precise U-Pb dating of zircon by laser ablation quadrupole ICP-MS. Geochemistry, Geophysics, Geosystems. 11(11), 1-12

Shaulis, B.J., Righter, M., Lapen, T.J., Jolliff, B.L., and Irving, A.J., (2017) 3.1 Ga crystallization age for magnesian and ferroan gabbro lithologies in the Northwest Africa 773 clan of lunar meteorites. Geochimica et Cosmochimica Acta. 213, 435-456

Waples, D. W., and Waples, J. S. (2004). A Review and Evaluation of Specific Heat Capacities of Rocks, Minerals, and Subsurface Fluids. Part 1: Minerals and Nonporous Rocks. Natural Resources Research, 13(2), 97–122.

Wiedenbeck, M., Hanchar, J. M., Peck, W. H., Sylvester, P., Valley, J., Whitehouse, M., ... & Zheng, Y. F. (2004). Further characterisation of the 91500 zircon crystal. Geostandards and Geoanalytical Research, 28(1), 9-39.

# Tables

## Table S1

Sanidine simulation parameters for Mie-Grüneisen EoS

| **Material properties used for simulating sanidine** | **Simulation (Figure 10) settings** | **Source** |
|---|---|---|
| Density | 2.58 g/cm$^3$ | Wapels and Wapels, 2004 |
| Grüneisen parameter (plag feldspar) | 0.42 | Tribaudino et al., (2011) |
| Speed of sound in sanidine | $3.10\times10^3$ m/s | Ahrens and Johnson, 1994 |
| U-Up constant | 1.39 | Ahrens and Johnson, 1994 |
| $C_p$ for sanidine calculated at 1000 ºC | 1164 J/(kg sanidine × T[in K]) | Hemingway et al., (1981). |

## Table S2

LA-ICP-MS major wt% element results for unshocked and post-shock sanidine

| | Al weight % | Al weight % 2 s.e. | K weight % | K weight % 2 s.e. |
|---|---|---|---|---|
| **Unshocked** | | | | |
| Sanidine A – 5 spot average | 10.84 | 0.34 | 9.716 | 0.29 |
| Sanidine B – 6 spot average | 10.78 | 0.19 | 9.617 | 0.15 |
| **Shocked** | | | | |
| Sanidine-average of 8 LA-ICP-MS spots | 10.05 | 0.22 | 10.29 | 0.23 |

Error in 2 s.e.

## Table S3

LA-ICP-MS results from individual analyses (VT=Vertical Transverse, HT=Additional data from Horizontal Transverse)

| **LA-ICP-MS** | | | **207Pb/235U** | 2 s.e. | **206Pb/238U** | 2 s.e. | **207Pb/206Pb** | 2 s.e. |
|---|---|---|---|---|---|---|---|---|
| ReiditeGrA | | Reidite | **1.855** | 5.49E-02 | **0.178** | 4.13E-03 | **0.076** | 1.59E-03 |
| **VT-1** | Vertical Transverse | Zircon | **1.872** | 3.87E-02 | **0.178** | 2.33E-03 | **0.076** | 1.40E-03 |
| **VT-2** | Vertical Transverse | Zircon | **1.822** | 3.15E-02 | **0.178** | 2.47E-03 | **0.074** | 1.30E-03 |
| **VT-3** | Vertical Transverse | Zircon | **1.835** | 3.72E-02 | **0.179** | 2.75E-03 | **0.075** | 1.40E-03 |
| **VT-4** | Vertical Transverse | Zircon | **1.804** | 3.37E-02 | **0.176** | 2.61E-03 | **0.075** | 1.49E-03 |
| **VT-5** | Vertical Transverse | Zircon | **1.856** | 3.74E-02 | **0.179** | 2.47E-03 | **0.075** | 1.30E-03 |
| **VT-6** | Vertical Transverse | Zircon | **1.802** | 3.57E-02 | **0.176** | 2.33E-03 | **0.074** | 1.40E-03 |
| **VT-7** | Vertical Transverse | Zircon | **1.817** | 3.44E-02 | **0.177** | 2.61E-03 | **0.074** | 1.30E-03 |
| **VT-8** | Vertical Transverse | Zircon | **1.830** | 4.02E-02 | **0.179** | 2.47E-03 | **0.074** | 1.59E-03 |
| **VT-9** | Vertical Transverse | Zircon | **1.831** | 2.89E-02 | **0.178** | 2.06E-03 | **0.075** | 9.77E-04 |
| **VT-10** | Vertical Transverse | Zircon | **1.867** | 2.92E-02 | **0.179** | 2.47E-03 | **0.076** | 1.01E-03 |
| **VT-11** | Vertical Transverse | Zircon | **1.842** | 3.32E-02 | **0.178** | 2.20E-03 | **0.075** | 1.20E-03 |
| **VT-12** | Vertical Transverse | Zircon | **1.850** | 3.03E-02 | **0.179** | 2.20E-03 | **0.075** | 1.30E-03 |
| **VT-13** | Vertical Transverse | Zircon | **1.863** | 3.33E-02 | **0.180** | 2.34E-03 | **0.075** | 1.20E-03 |
| **VT-14** | Vertical Transverse | Zircon | **1.832** | 3.46E-02 | **0.177** | 2.20E-03 | **0.075** | 1.40E-03 |
| **VT-15** | Vertical Transverse | Zircon | **1.866** | 3.32E-02 | **0.180** | 2.34E-03 | **0.075** | 1.20E-03 |
| **VT-16** | Vertical Transverse | Zircon | **1.858** | 3.29E-02 | **0.178** | 2.62E-03 | **0.076** | 1.10E-03 |
| **HT-1** | Horizontal Transverse | Zircon | **1.830** | 4.14E-02 | **0.176** | 2.48E-03 | **0.075** | 1.79E-03 |
| **HT-2** | Horizontal Transverse | Zircon | **1.870** | 3.89E-02 | **0.178** | 2.48E-03 | **0.076** | 1.59E-03 |
| **HT-3** | Horizontal Transverse | Zircon | **1.818** | 4.64E-02 | **0.175** | 2.89E-03 | **0.075** | 1.89E-03 |
| **HT-4** | Horizontal Transverse | Zircon | **1.865** | 3.47E-02 | **0.182** | 2.34E-03 | **0.074** | 1.20E-03 |
| **HT-5** | Horizontal Transverse | Zircon | **1.825** | 3.18E-02 | **0.177** | 2.20E-03 | **0.075** | 1.40E-03 |
| **HT-6** | Horizontal Transverse | Zircon | **1.844** | 3.76E-02 | **0.179** | 2.48E-03 | **0.075** | 1.59E-03 |

| **LA-ICP-MS** | | **207Pb/206Pb (Age (Ma))** | 2 s.e. | **207Pb/235U (Age (Ma))** | 2 s.e. | **206Pb/238U (Age (Ma))** | 2 s.e. |
|---|---|---|---|---|---|---|---|
| ReiditeGrA | Reidite | 1082 | 42.3 | 1065 | **19.5** | 1058 | **22.6** |
| **VT-1** | Zircon | 1100 | 36.7 | 1071 | **13.7** | 1058 | **12.8** |
| **VT-2** | Zircon | 1053 | 35.1 | 1053 | **11.3** | 1054 | **13.5** |
| **VT-3** | Zircon | 1056 | 37.7 | 1058 | **13.3** | 1060 | **15.0** |
| **VT-4** | Zircon | 1056 | 40.4 | 1047 | **12.2** | 1043 | **14.3** |
| **VT-5** | Zircon | 1080 | 34.6 | 1066 | **13.3** | 1060 | **13.5** |
| **VT-6** | Zircon | 1045 | 38.0 | 1046 | **12.9** | 1048 | **12.8** |
| **VT-7** | Zircon | 1050 | 35.2 | 1052 | **12.4** | 1053 | **14.3** |
| **VT-8** | Zircon | 1050 | 43.2 | 1056 | **14.4** | 1060 | **13.5** |
| **VT-9** | Zircon | 1061 | 26.3 | 1057 | **10.4** | 1056 | **11.3** |
| **VT-10** | Zircon | 1082 | 26.7 | 1070 | **10.3** | 1064 | **13.5** |
| **VT-11** | Zircon | 1072 | 32.1 | 1060 | **11.8** | 1056 | **12.0** |
| **VT-12** | Zircon | 1069 | 34.8 | 1063 | **10.8** | 1061 | **12.0** |
| **VT-13** | Zircon | 1072 | 32.1 | 1068 | **11.8** | 1067 | **12.8** |
| **VT-14** | Zircon | 1066 | 37.5 | 1057 | **12.4** | 1053 | **12.1** |
| **VT-15** | Zircon | 1074 | 32.1 | 1069 | **11.7** | 1067 | **12.8** |
| **VT-16** | Zircon | 1085 | 29.3 | 1066 | **11.7** | 1058 | **14.3** |
| **HT-1** | Zircon | 1080 | 47.6 | 1056 | **14.9** | 1046 | **13.6** |
| **HT-2** | Zircon | 1103 | 41.7 | 1070 | **13.8** | 1055 | **13.6** |
| **HT-3** | Zircon | 1074 | 50.4 | 1052 | **16.7** | 1042 | **15.9** |
| **HT-4** | Zircon | 1048 | 32.6 | 1069 | **12.3** | 1080 | **12.8** |
| **HT-5** | Zircon | 1061 | 37.6 | 1054 | **11.4** | 1052 | **12.1** |
| **HT-6** | Zircon | 1056 | 43.0 | 1061 | **13.4** | 1065 | **13.6** |

| **LA-ICP-MS** | | **U ppm** | 2 s.e. | **Th ppm** | 2 s.e. | **Dα** | **dpa** |
|---|---|---|---|---|---|---|---|
| ReiditeGrA | Reidite | **146** | 2.15 | **47** | 0.63 | **6.08E+15** | **0.29** |
| **VT-1** | Zircon | **150** | 2.91 | **54** | 0.63 | **6.41E+15** | **0.31** |
| **VT-2** | Zircon | **134** | 2.53 | **46** | 0.63 | **5.47E+15** | **0.26** |
| **VT-3** | Zircon | **128** | 2.05 | **39** | 0.44 | **5.2E+15** | **0.25** |
| **VT-4** | Zircon | **152** | 2.96 | **49** | 0.68 | **6.21E+15** | **0.30** |
| **VT-5** | Zircon | **154** | 2.63 | **50** | 0.57 | **6.43E+15** | **0.31** |
| **VT-6** | Zircon | **162** | 2.77 | **54** | 0.57 | **6.56E+15** | **0.31** |
| **VT-7** | Zircon | **158** | 2.72 | **52** | 0.63 | **6.4E+15** | **0.31** |
| **VT-8** | Zircon | **112** | 2.01 | **29** | 0.43 | **4.48E+15** | **0.21** |
| **VT-9** | Zircon | **264** | 4.21 | **81** | 0.84 | **1.08E+16** | **0.51** |
| **VT-10** | Zircon | **242** | 7.17 | **74** | 2.19 | **1.01E+16** | **0.48** |
| **VT-11** | Zircon | **241** | 2.96 | **73** | 0.57 | **9.94E+15** | **0.47** |
| **VT-12** | Zircon | **187** | 2.53 | **50** | 0.50 | **7.62E+15** | **0.36** |
| **VT-13** | Zircon | **206** | 1.96 | **49** | 0.43 | **8.39E+15** | **0.40** |
| **VT-14** | Zircon | **203** | 3.25 | **56** | 0.68 | **8.27E+15** | **0.39** |
| **VT-15** | Zircon | **210** | 5.73 | **60** | 1.78 | **8.64E+15** | **0.41** |
| **VT-16** | Zircon | **224** | 3.54 | **53** | 0.63 | **9.22E+15** | **0.44** |
| **HT-1** | Zircon | **106** | 2.10 | **28** | 0.41 | **4.35E+15** | **0.21** |
| **HT-2** | Zircon | **121** | 2.10 | **34** | 0.47 | **5.14E+15** | **0.24** |
| **HT-3** | Zircon | **97** | 1.82 | **26** | 0.31 | **3.99E+15** | **0.19** |
| **HT-4** | Zircon | **170** | 3.34 | **57** | 0.84 | **6.9E+15** | **0.33** |
| **HT-5** | Zircon | **171** | 3.25 | **57** | 0.78 | **7.04E+15** | **0.34** |
| **HT-6** | Zircon | **157** | 2.96 | **50** | 0.68 | **6.41E+15** | **0.31** |

## Table S4

SIMS results from individual analyses on zircon, reidite and metamict $ZrSiO_4$

| SIMS | Notes | Measurement | 207Pb/235U | 207Pb/235U | 206Pb/238U | 206Pb/238U | 207Pb/206Pb | 207Pb/206Pb |
|---|---|---|---|---|---|---|---|---|
| | | | Value | 1 s.e. | Value | 1 s.e. | Value | 2 s.e. |
| U-Pb-July2021\ KLr@1.ais | | Reidite | 1.95E+00 | 8.28E-02 | 1.77E-01 | 4.21E-03 | 8.01E-02 | 2.16E-03 |
| U-Pb-July2021\ KLr@10.ais | | Reidite | 1.81E+00 | 7.52E-02 | 1.85E-01 | 5.62E-03 | 7.10E-02 | 2.57E-03 |
| U-Pb-July2021\ KLr@11.ais | | Reidite | 1.79E+00 | 6.86E-02 | 1.84E-01 | 4.30E-03 | 7.08E-02 | 2.15E-03 |
| U-Pb-July2021\ KLr@2.ais | | Reidite | 1.77E+00 | 8.48E-02 | 1.80E-01 | 3.88E-03 | 7.11E-02 | 3.28E-03 |
| U-Pb-July2021\ KLr@3.ais | | Reidite | 1.79E+00 | 9.63E-02 | 1.78E-01 | 4.86E-03 | 7.27E-02 | 3.09E-03 |
| U-Pb-July2021\ KLr@4.ais | | Reidite | 1.83E+00 | 8.65E-02 | 1.81E-01 | 4.96E-03 | 7.33E-02 | 3.39E-03 |
| U-Pb-July2021\ KLr@5.ais | | Reidite | 1.83E+00 | 8.52E-02 | 1.85E-01 | 4.51E-03 | 7.17E-02 | 2.29E-03 |
| U-Pb-July2021\ KLr@7.ais | | Reidite | 1.83E+00 | 9.91E-02 | 1.71E-01 | 4.55E-03 | 7.73E-02 | 3.46E-03 |
| U-Pb-July2021\ KLr@8.ais | | Reidite | 1.86E+00 | 8.06E-02 | 1.73E-01 | 3.96E-03 | 7.78E-02 | 2.49E-03 |
| U-Pb-July2021\ KLr@9.ais | | Reidite | 1.69E+00 | 9.54E-02 | 1.74E-01 | 3.86E-03 | 7.03E-02 | 3.28E-03 |
| U-Pb-July2021\ KLz@1.ais | | Zircon | 1.81E+00 | 6.05E-02 | 1.78E-01 | 4.52E-03 | 7.36E-02 | 1.70E-03 |
| U-Pb-July2021\ KLz@10.ais | | Zircon | 1.83E+00 | 9.01E-02 | 1.80E-01 | 4.25E-03 | 7.40E-02 | 3.36E-03 |
| U-Pb-July2021\ KLz@2.ais | | Zircon | 1.84E+00 | 6.29E-02 | 1.82E-01 | 4.07E-03 | 7.33E-02 | 1.70E-03 |
| U-Pb-July2021\ KLz@3.ais | | Zircon | 1.81E+00 | 5.81E-02 | 1.83E-01 | 4.05E-03 | 7.21E-02 | 2.02E-03 |
| U-Pb-July2021\ KLz@4.ais | | Zircon | 1.87E+00 | 6.77E-02 | 1.79E-01 | 3.87E-03 | 7.55E-02 | 1.81E-03 |
| U-Pb-July2021\ KLz@5.ais | | Zircon | 1.93E+00 | 6.91E-02 | 1.81E-01 | 4.25E-03 | 7.72E-02 | 1.61E-03 |
| U-Pb-July2021\ KLz@6.ais | | Zircon | 1.86E+00 | 6.86E-02 | 1.84E-01 | 4.28E-03 | 7.37E-02 | 1.64E-03 |
| U-Pb-July2021\ KLz@7.ais | | Zircon | 1.87E+00 | 5.10E-02 | 1.82E-01 | 3.95E-03 | 7.42E-02 | 1.53E-03 |
| U-Pb-July2021\ KLz@8.ais | | Zircon | 1.80E+00 | 4.63E-02 | 1.77E-01 | 4.54E-03 | 7.38E-02 | 1.33E-03 |
| U-Pb-July2021\ KLz@9.ais | | Zircon | 1.82E+00 | 5.96E-02 | 1.78E-01 | 4.00E-03 | 7.43E-02 | 1.64E-03 |
| U-Pb-July2021\ Klzm@1.ais | | ZrSiO4 | 1.63E+00 | 3.73E-02 | 1.59E-01 | 3.83E-03 | 7.42E-02 | 4.53E-04 |
| U-Pb-July2021\ Klzm@2.ais | | ZrSiO4 | 1.89E+00 | 3.59E-02 | 1.84E-01 | 3.75E-03 | 7.46E-02 | 3.47E-04 |
| U-Pb-July2021\ Klzm@3.ais | | ZrSiO4 | 1.85E+00 | 3.42E-02 | 1.79E-01 | 3.51E-03 | 7.50E-02 | 4.39E-04 |
| U-Pb-July2021\ KLzm@4.ais | | ZrSiO4 | 1.85E+00 | 4.28E-02 | 1.80E-01 | 4.15E-03 | 7.47E-02 | 3.19E-04 |
| U-Pb-July2021\ KLzm@5.ais | | ZrSiO4 | 1.84E+00 | 8.11E-02 | 1.81E-01 | 4.16E-03 | 7.40E-02 | 2.09E-03 |
| U-Pb-July2021\ KLzm@6.ais | shallow | ZrSiO4a | 1.59E+00 | 8.79E-02 | 1.54E-01 | 9.03E-03 | 7.46E-02 | 2.74E-04 |
| U-Pb-July2021\ KLzm@6.ais | deep | ZrSiO4b | 2.07E+00 | 2.01E-01 | 1.83E-01 | 1.64E-02 | 8.22E-02 | 1.80E-03 |
| U-Pb-July2021\ KLzm@6.ais | all data | ZrSiO4c | 1.88E+00 | 1.40E-01 | 1.72E-01 | 9.78E-03 | 7.93E-02 | 1.90E-03 |
| U-Pb-July2021\ KLzm@7.ais | | ZrSiO4 | 1.79E+00 | 7.56E-02 | 1.73E-01 | 7.35E-03 | 7.47E-02 | 3.85E-04 |

| **SIMS** | Measurement | 207Pb/206Pb | 207Pb/206Pb | 207Pb/235U | 207Pb/235U | 206Pb/238U | 206Pb/238U |
|---|---|---|---|---|---|---|---|
| | | Age (Ma) | ±1 s.e. | Age (Ma) | ±1 s.e. | Age (Ma) | ±1 s.e. |
| U-Pb-July2021\ KLr@1.ais | Reidite | 1199 | 53 | 1098 | 29 | 1048 | 23 |
| U-Pb-July2021\ KLr@10.ais | Reidite | 957 | 74 | 1049 | 27 | 1093 | 31 |
| U-Pb-July2021\ KLr@11.ais | Reidite | 951 | 62 | 1043 | 25 | 1088 | 23 |
| U-Pb-July2021\ KLr@2.ais | Reidite | 961 | 94 | 1033 | 31 | 1067 | 21 |
| U-Pb-July2021\ KLr@3.ais | Reidite | 1005 | 86 | 1041 | 35 | 1058 | 27 |
| U-Pb-July2021\ KLr@4.ais | Reidite | 1023 | 94 | 1054 | 31 | 1070 | 27 |
| U-Pb-July2021\ KLr@5.ais | Reidite | 978 | 65 | 1057 | 31 | 1097 | 25 |
| U-Pb-July2021\ KLr@7.ais | Reidite | 1130 | 89 | 1055 | 36 | 1020 | 25 |
| U-Pb-July2021\ KLr@8.ais | Reidite | 1141 | 64 | 1066 | 29 | 1030 | 22 |
| U-Pb-July2021\ KLr@9.ais | Reidite | 936 | 96 | 1003 | 36 | 1034 | 21 |
| U-Pb-July2021\ KLz@1.ais | Zircon | 1029 | 47 | 1048 | 22 | 1057 | 25 |
| U-Pb-July2021\ KLz@10.ais | Zircon | 1043 | 92 | 1057 | 32 | 1064 | 23 |
| U-Pb-July2021\ KLz@2.ais | Zircon | 1023 | 47 | 1061 | 22 | 1080 | 22 |
| U-Pb-July2021\ KLz@3.ais | Zircon | 988 | 57 | 1051 | 21 | 1081 | 22 |
| U-Pb-July2021\ KLz@4.ais | Zircon | 1082 | 48 | 1070 | 24 | 1064 | 21 |
| U-Pb-July2021\ KLz@5.ais | Zircon | 1127 | 41 | 1091 | 24 | 1073 | 23 |
| U-Pb-July2021\ KLz@6.ais | Zircon | 1032 | 45 | 1068 | 24 | 1086 | 23 |
| U-Pb-July2021\ KLz@7.ais | Zircon | 1048 | 42 | 1069 | 18 | 1080 | 22 |
| U-Pb-July2021\ KLz@8.ais | Zircon | 1037 | 36 | 1046 | 17 | 1050 | 25 |
| U-Pb-July2021\ KLz@9.ais | Zircon | 1049 | 44 | 1053 | 21 | 1055 | 22 |
| U-Pb-July2021\ Klzm@1.ais | ZrSiO4 | 1046 | 12 | 980 | 14 | 951 | 21 |
| U-Pb-July2021\ Klzm@2.ais | ZrSiO4 | 1056 | 9 | 1076 | 13 | 1086 | 20 |
| U-Pb-July2021\ Klzm@3.ais | ZrSiO4 | 1067 | 12 | 1062 | 12 | 1060 | 19 |
| U-Pb-July2021\ KLzm@4.ais | ZrSiO4 | 1061 | 9 | 1063 | 15 | 1064 | 23 |
| U-Pb-July2021\ KLzm@5.ais | ZrSiO4 | 1041 | 57 | 1060 | 29 | 1070 | 23 |
| U-Pb-July2021\ KLzm@6.ais | ZrSiO4a | 1059 | 7 | 964 | 35 | 923 | 50 |
| U-Pb-July2021\ KLzm@6.ais | ZrSiO4b | 1251 | 43 | 1140 | 66 | 1082 | 89 |
| U-Pb-July2021\ KLzm@6.ais | ZrSiO4c | 1180 | 47 | 1075 | 49 | 1024 | 54 |
| U-Pb-July2021\ KLzm@7.ais | ZrSiO4 | 1060 | 10 | 1040 | 28 | 1030 | 40 |

| SIMS | Measurement | U ppm | U ppm | Th ppm | Th ppm | Dα | dpa |
|---|---|---|---|---|---|---|---|
| | | Value | ±1 s.d. | Value | ±1 s.d. | | |
| U-Pb-July2021\ KLr@1.ais | Reidite | 72 | 7 | 24 | 3 | 3.37E+15 | 0.16 |
| U-Pb-July2021\ KLr@10.ais | Reidite | 61 | 6 | 19 | 2 | 2.24E+15 | 0.11 |
| U-Pb-July2021\ KLr@11.ais | Reidite | 91 | 14 | 32 | 4 | 3.34E+15 | 0.16 |
| U-Pb-July2021\ KLr@2.ais | Reidite | 62 | 6 | 20 | 2 | 2.31E+15 | 0.11 |
| U-Pb-July2021\ KLr@3.ais | Reidite | 60 | 6 | 20 | 2 | 2.32E+15 | 0.11 |
| U-Pb-July2021\ KLr@4.ais | Reidite | 57 | 6 | 19 | 2 | 2.25E+15 | 0.11 |
| U-Pb-July2021\ KLr@5.ais | Reidite | 53 | 5 | 17 | 2 | 2.00E+15 | 0.10 |
| U-Pb-July2021\ KLr@7.ais | Reidite | 54 | 5 | 18 | 2 | 2.37E+15 | 0.11 |
| U-Pb-July2021\ KLr@8.ais | Reidite | 53 | 5 | 18 | 2 | 2.35E+15 | 0.11 |
| U-Pb-July2021\ KLr@9.ais | Reidite | 53 | 5 | 17 | 2 | 1.92E+15 | 0.09 |
| U-Pb-July2021\ KLz@1.ais | Zircon | 79 | 8 | 21 | 2 | 3.10E+15 | 0.15 |
| U-Pb-July2021\ KLz@10.ais | Zircon | 55 | 6 | 15 | 2 | 2.18E+15 | 0.10 |
| U-Pb-July2021\ KLz@2.ais | Zircon | 104 | 11 | 29 | 3 | 4.08E+15 | 0.19 |
| U-Pb-July2021\ KLz@3.ais | Zircon | 108 | 11 | 29 | 3 | 4.07E+15 | 0.19 |
| U-Pb-July2021\ KLz@4.ais | Zircon | 104 | 11 | 29 | 4 | 4.32E+15 | 0.21 |
| U-Pb-July2021\ KLz@5.ais | Zircon | 95 | 10 | 27 | 3 | 4.10E+15 | 0.20 |
| U-Pb-July2021\ KLz@6.ais | Zircon | 115 | 12 | 34 | 4 | 4.56E+15 | 0.22 |
| U-Pb-July2021\ KLz@7.ais | Zircon | 124 | 13 | 40 | 5 | 5.02E+15 | 0.24 |
| U-Pb-July2021\ KLz@8.ais | Zircon | 103 | 11 | 30 | 4 | 4.10E+15 | 0.20 |
| U-Pb-July2021\ KLz@9.ais | Zircon | 118 | 12 | 35 | 4 | 4.77E+15 | 0.23 |
| U-Pb-July2021\ Klzm@1.ais | ZrSiO4 | 2643 | 299 | 433 | 51 | 1.03E+17 | 4.93 |
| U-Pb-July2021\ Klzm@2.ais | ZrSiO4 | 3250 | 343 | 338 | 42 | 1.27E+17 | 6.04 |
| U-Pb-July2021\ Klzm@3.ais | ZrSiO4 | 1431 | 147 | 396 | 54 | 5.84E+16 | 2.79 |
| U-Pb-July2021\ KLzm@4.ais | ZrSiO4 | 1911 | 196 | 318 | 38 | 7.58E+16 | 3.62 |
| U-Pb-July2021\ KLzm@5.ais | ZrSiO4 | 1391 | 141 | 846 | 99 | 5.92E+16 | 2.82 |
| U-Pb-July2021\ KLzm@6.ais | ZrSiO4a | 2873 | 291 | 447 | 55 | 1.13E+17 | 5.41 |
| U-Pb-July2021\ KLzm@6.ais | ZrSiO4b | 2266 | 251 | 478 | 56 | 1.08E+17 | 5.13 |
| U-Pb-July2021\ KLzm@6.ais | ZrSiO4c | 2509 | 273 | 475 | 56 | 1.12E+17 | 5.32 |
| U-Pb-July2021\ KLzm@7.ais | ZrSiO4 | 2585 | 263 | 1442 | 203 | 1.11E+17 | 5.29 |

## Table S5

Individual SIMS analyses of sanidine

| SIMS | 206Pb /204Pb | 206Pb /204Pb | 207Pb /204Pb | 207Pb /204Pb | 208Pb /204Pb | 208Pb /204Pb | 204Pb | 206Pb | 207Pb | 208Pb | 207Pb /206Pb | 207Pb /206Pb |
|---|---|---|---|---|---|---|---|---|---|---|---|---|
| | | 1 s.e. | | 1 s.e. | | 1 s.e. | | | | | | 1 s.e. |
| Sanidine | 1.88 E+01 | 3.06 E-01 | 1.54 E+01 | 2.49 E-01 | 3.85 E+01 | 6.09 E-01 | 7.58 E+01 | 1.43 E+03 | 1.17 E+03 | 2.91 E+03 | 8.20 E-01 | 7.15 E-03 |
| Sanidine | 1.89 E+01 | 3.71 E-01 | 1.55 E+01 | 3.02 E-01 | 3.87 E+01 | 7.42 E-01 | 5.17 E+01 | 9.74 E+02 | 7.99 E+02 | 2.00 E+03 | 8.19 E-01 | 7.51 E-03 |
| Sanidine | 1.90 E+01 | 3.09 E-01 | 1.55 E+01 | 2.51 E-01 | 3.83 E+01 | 6.08 E-01 | 7.53 E+01 | 1.43 E+03 | 1.17 E+03 | 2.89 E+03 | 8.16 E-01 | 5.51 E-03 |
| Sanidine | 1.88 E+01 | 3.03 E-01 | 1.53 E+01 | 2.46 E-01 | 3.81 E+01 | 6.00 E-01 | 7.66 E+01 | 1.44 E+03 | 1.17 E+03 | 2.91 E+03 | 8.16 E-01 | 4.84 E-03 |

# Figures (Supplemental)

**Figure S1:**

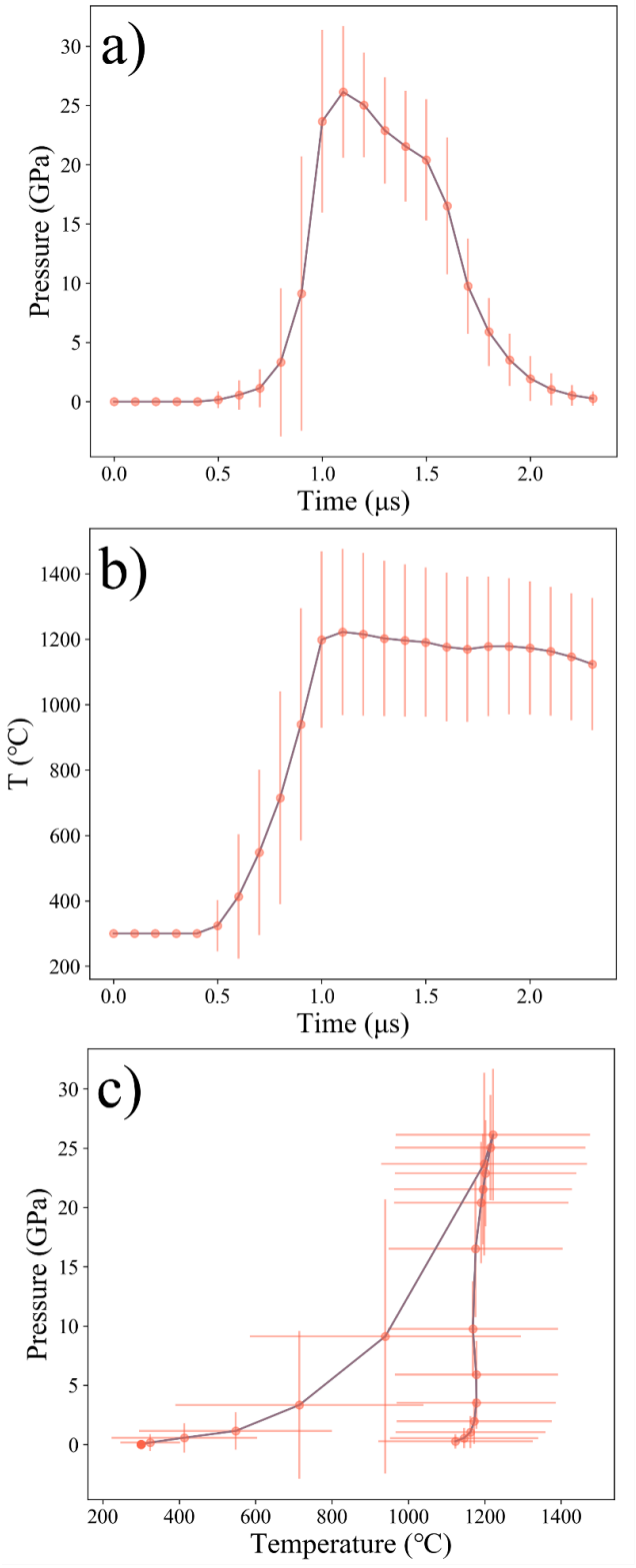

**Figure S1**, (**a**) *P*-Time profile of average pressure for all iSALE2D simulation tracers at each timestep in the experiment (**b**) T-Time profile of average pressure for iSALE2D simulation tracers across each timestep in the experiment (**c**) *P-T* graph of average pressure and average temperature for iSALE2D simulation tracers. For this panel, the initial experiment state is on the lower left where temperature is at 0 GPa and temperature is at 273 K.

**Figure S2:**

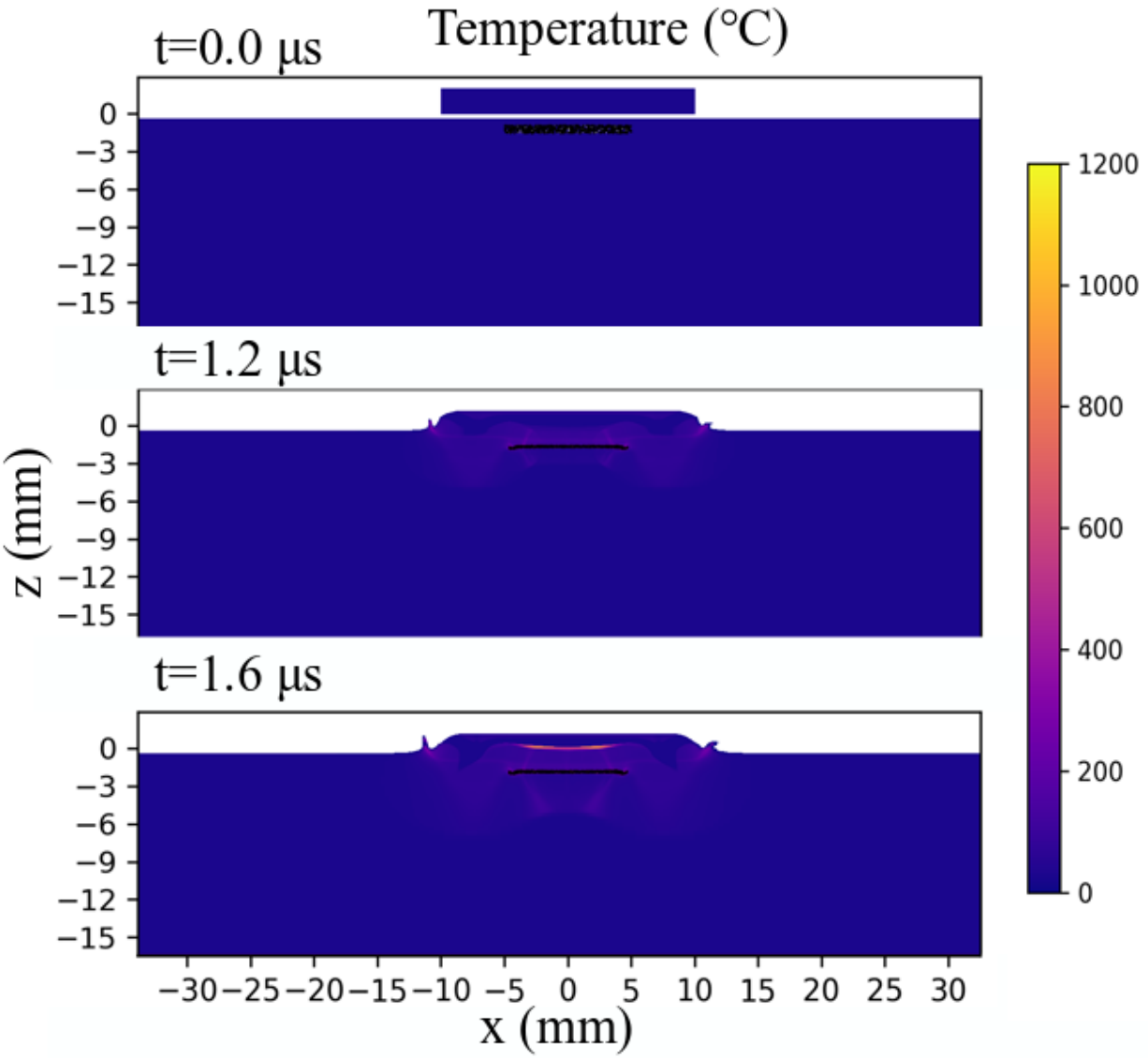


**Figure S2,** A version of **Figure 9a** in the text but with temperature plotted instead of pressure.

Figures S3-S5 are all animated .gif files. If they do not play inside this document, please see the corresponding .gif files which have been uploaded to the online repository as well.

**Figure S3a:**

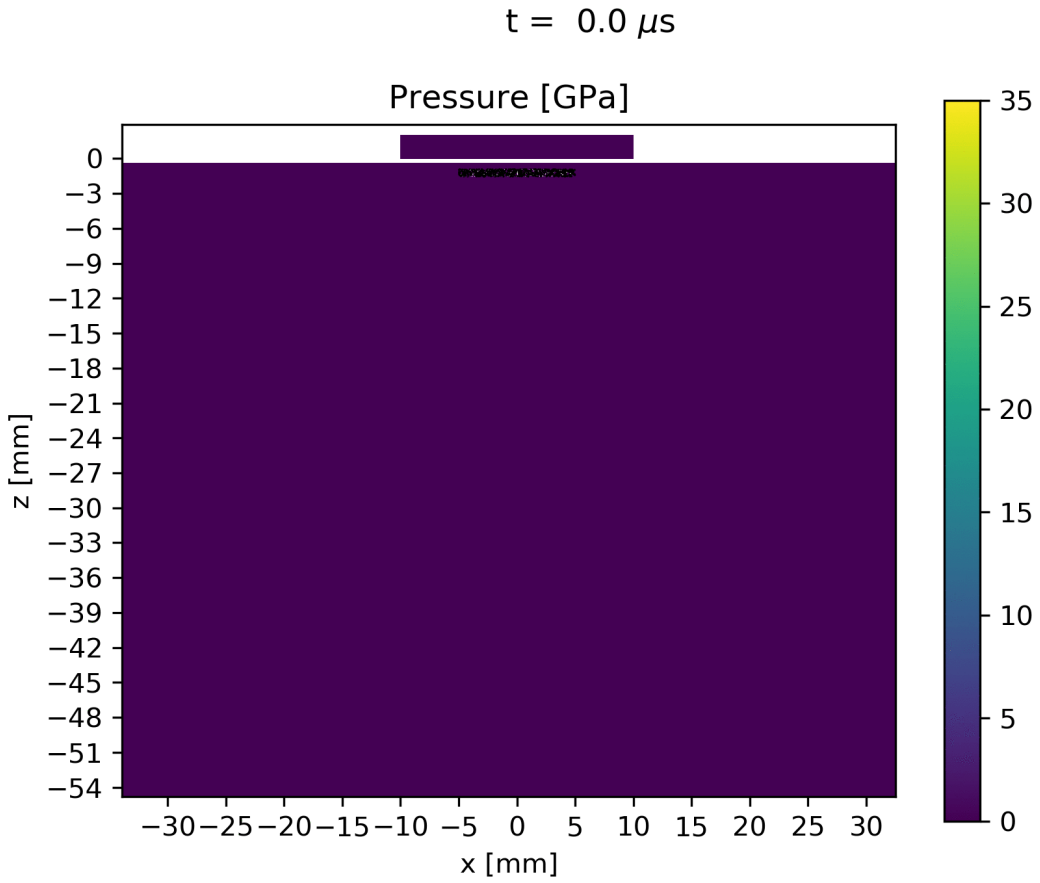


**Figure S3, (a)** An animated version of the iSALE2D simulation presented in **Figure 11a** in the text. The full scale allows the complete geometry of the simulation to be more easily understood.

**Figure S3b:**

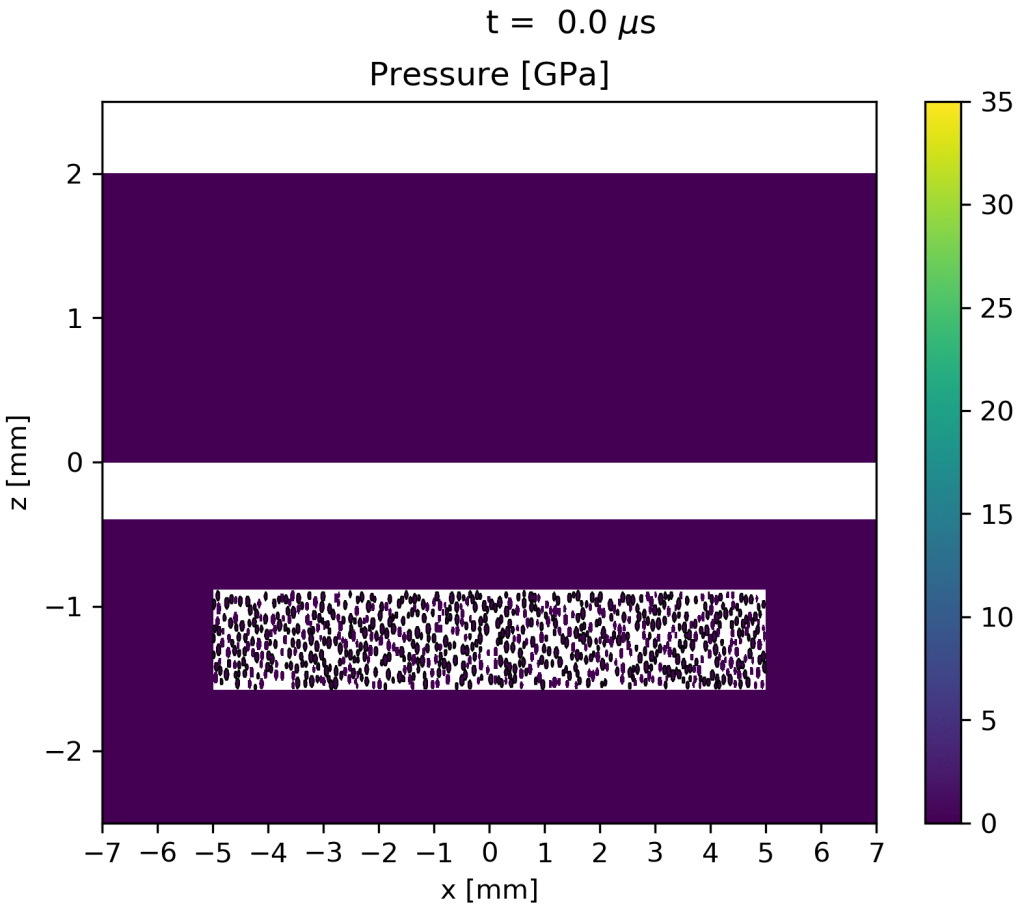


**Figure S3, (b)** An animated version of the iSALE2D simulation for pressure. This close-up version allows for an easier viewing of the pressures being experienced by the sample well.

**Figure S4:**

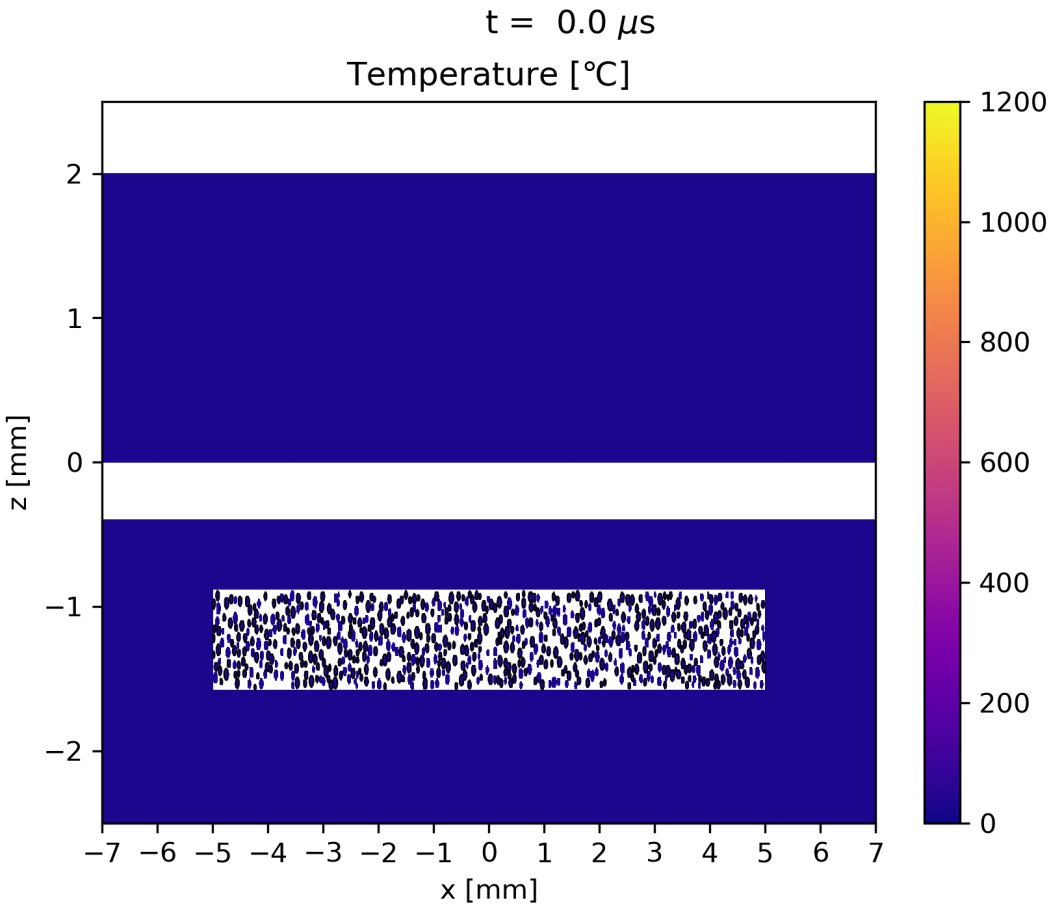


**Figure S4,** An animated version of the iSALE2D simulation for temperature. This close-up version focused on the sample well allows for an easier viewing of the temperatures experienced.

**Figure S5:**

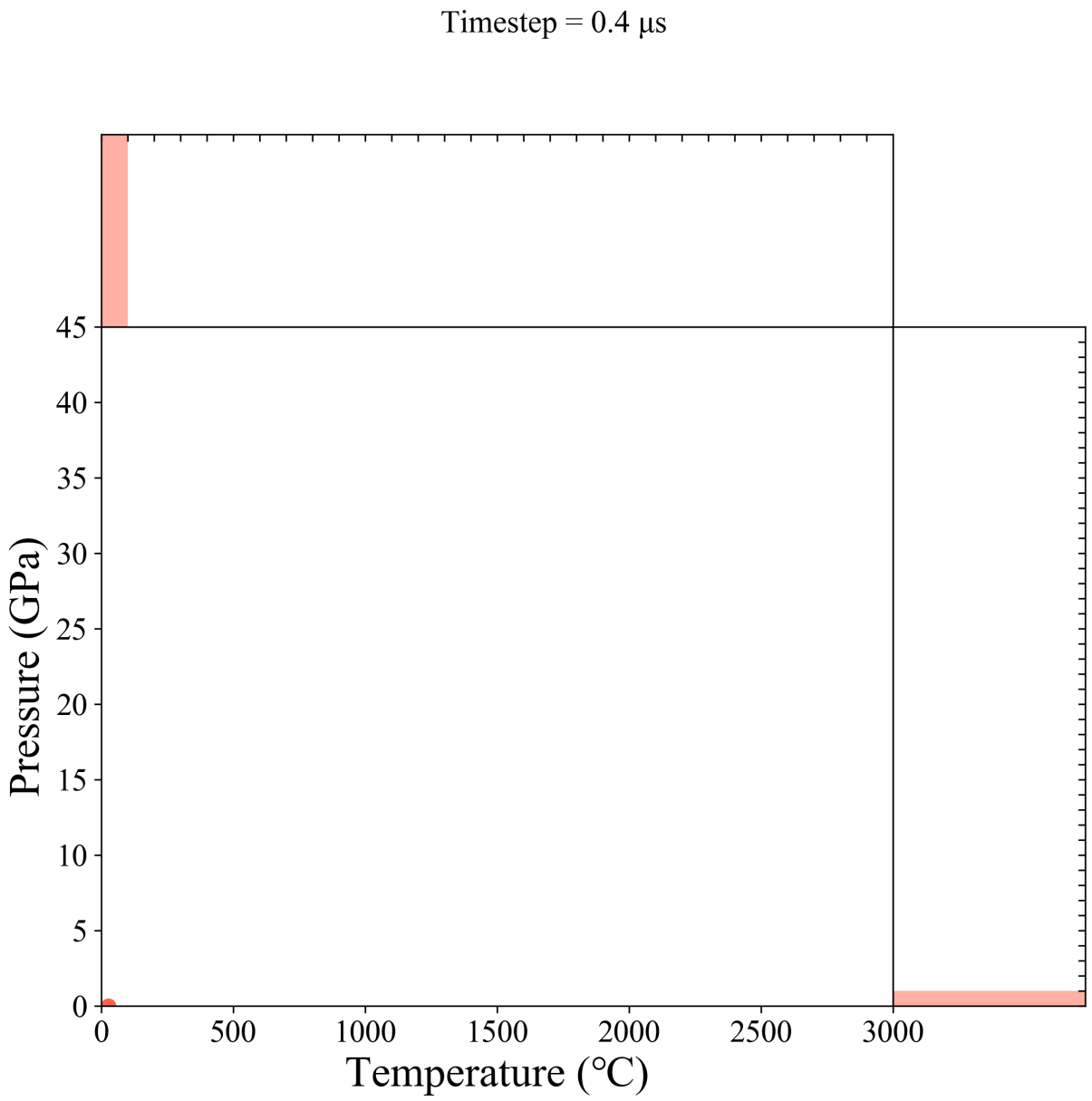


**Figure S5,** An animated plot showing the *P-T* tracer data from the simulation at every timestep from t=0.4 to t=2.3 μs.

**Figure S6:**

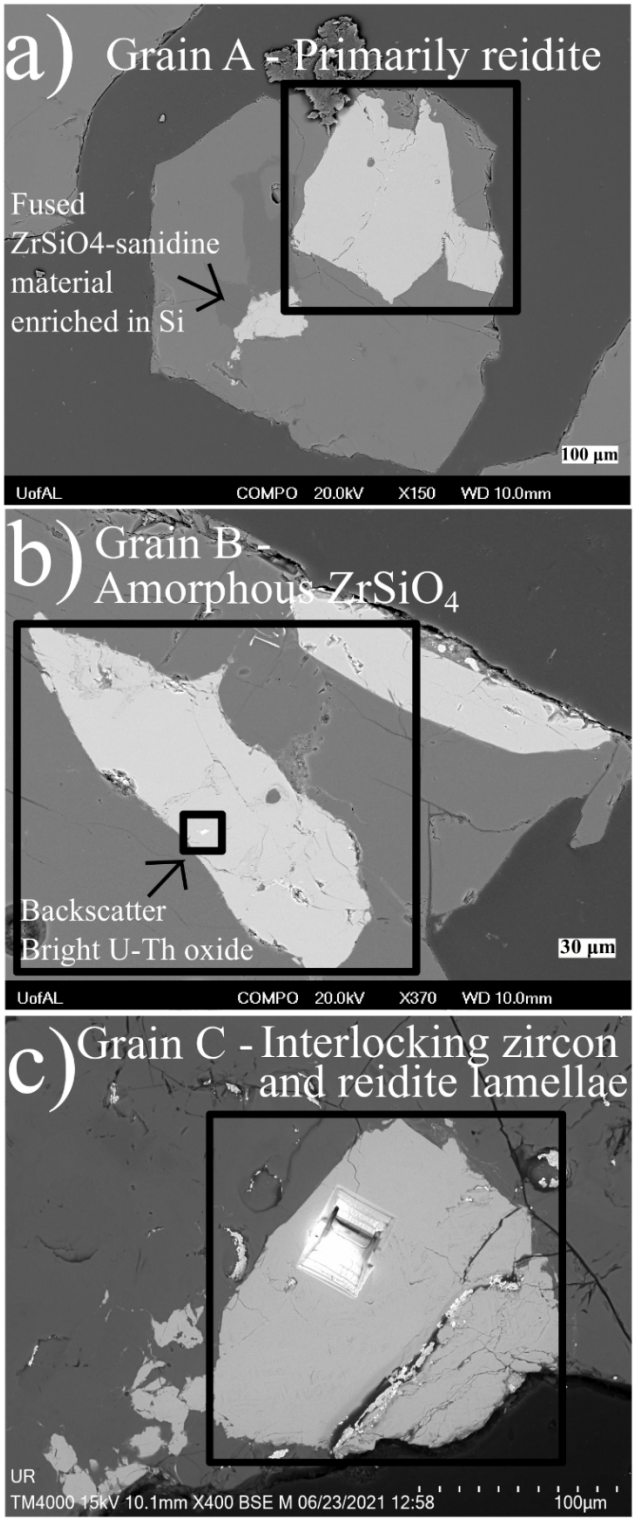
a) Grain A - Primarily reidite
Fused
ZrSiO4-sanidine
material
enriched in Si
100 µm
UofAL COMPO 20.0kV X150 WD 10.0mm
b) Grain B -
Amorphous ZrSiO4
Backscatter
Bright U-Th oxide
30 µm
UofAL COMPO 20.0kV X370 WD 10.0mm
c) Grain C - Interlocking zircon
and reidite lamellae
UR
TM4000 15kV 10.1mm X400 BSE M 06/23/2021 12:58
100µm

**Figure S6,** A replotting of Figure 1 from the main text with additional text information on each panel to aid in easy identification of regions or grains being discussed.

**Figure S7:**

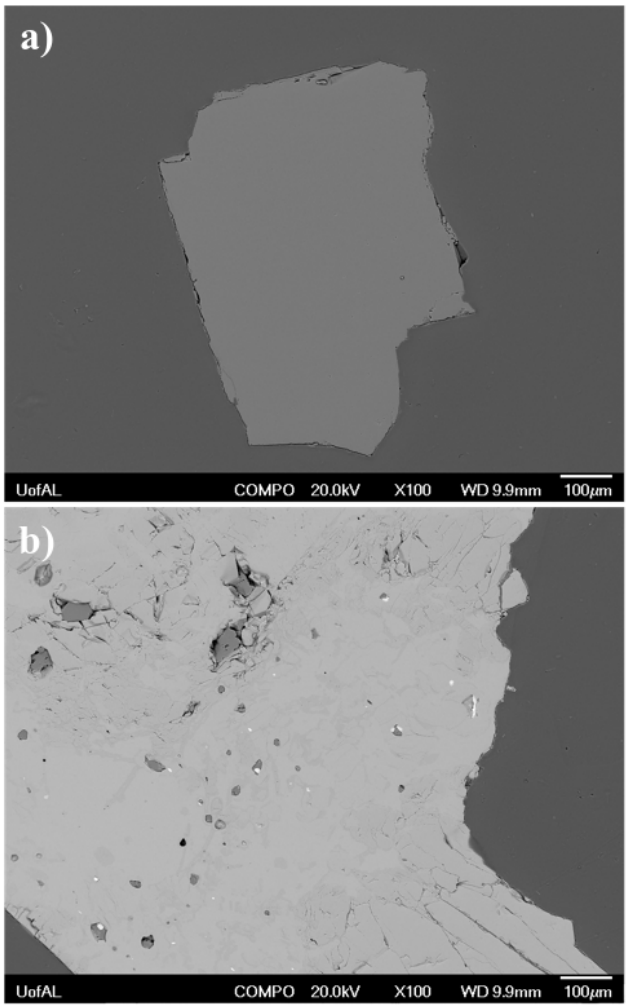
a)
UofAL COMPO 20.0kV X100 WD 9.9mm 100μm
b)
UofAL COMPO 20.0kV X100 WD 9.9mm 100μm

**Figure S7c:**

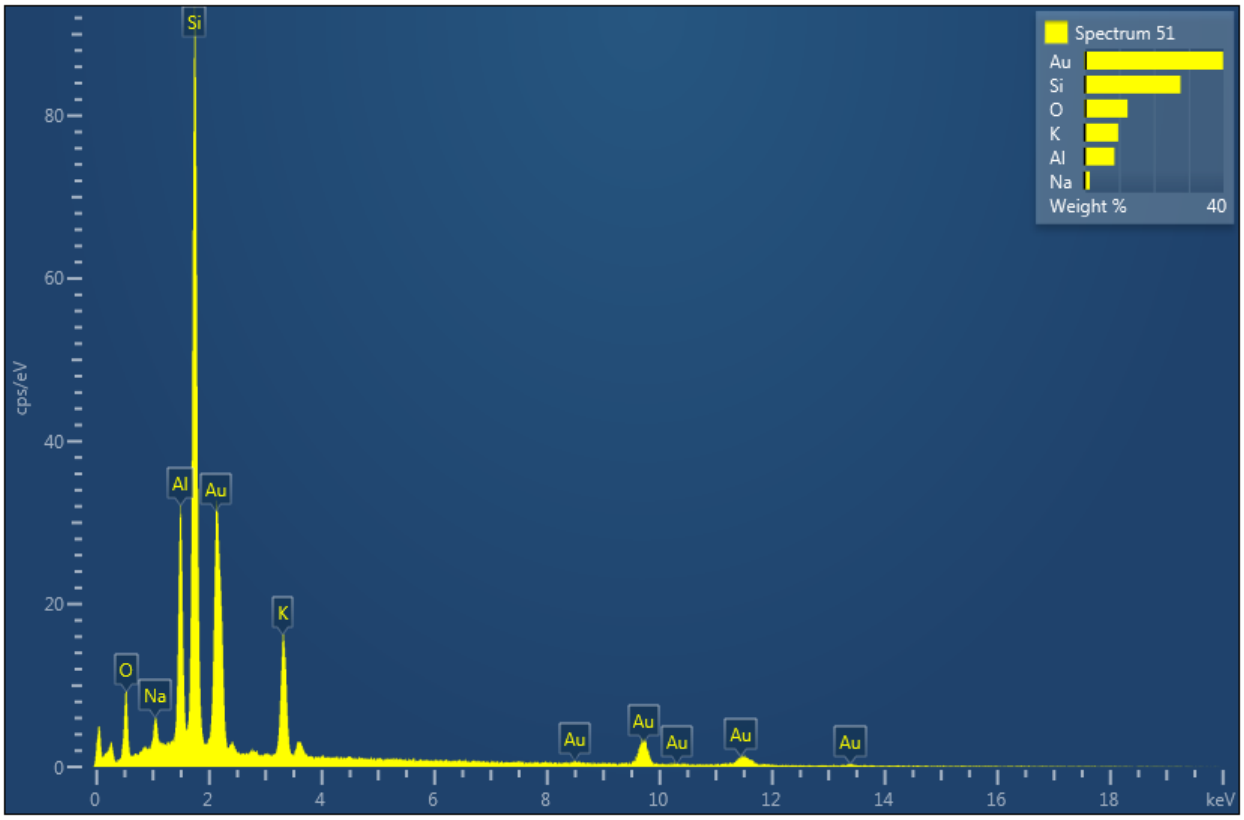
Spectrum 51
Au
Si
O
K
Al
Na
Weight %
40
cps/eV
0
20
40
60
80
Si
Al
Au
K
O
Na
Au
Au
Au
Au
Au
0
2
4
6
8
10
12
14
16
18
keV

**Figure S7d:**

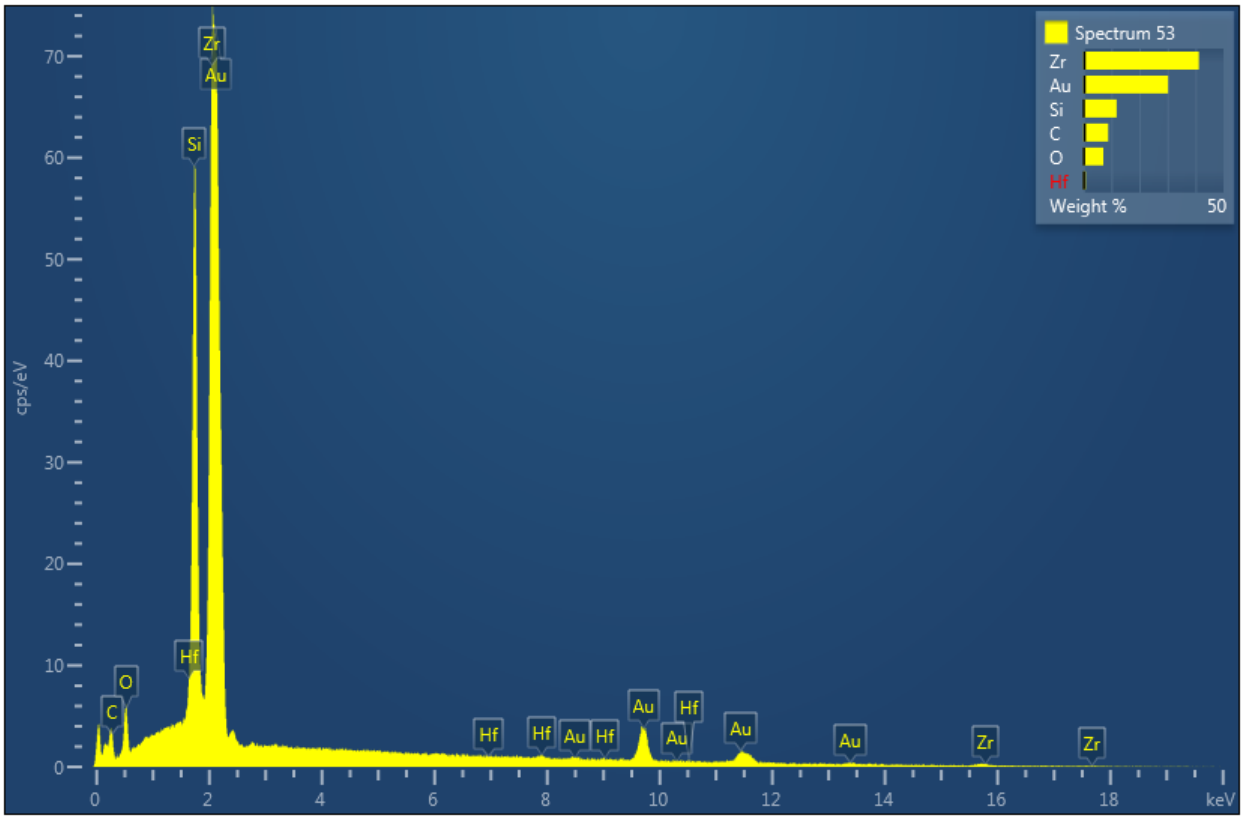


**Figure S7, (a)** BSE image showing a representative unshocked sanidine. **(b)** Unshocked zircon fragment sourced from the same hand sample as the zircon used in the shock experiment. The bright regions in BSE are U-Th oxide phases, commonly found present within zircons from this hand sample. **(c)** A representaive EDS spectrum of the unshocked sanidine. **(d)** A representative EDS spectrum of the unshocked zircon (avoiding both bright U-Th phases and darker regions). For both **(c)** and **(d)**, there is some recognition by the software of the Au coating on the sample. In all presented spectra, some peaks may be mislabeled as gold due to the presence of a gold coating to conduct electrons and how the software recognizes certain peaks.

**Figure S8:**

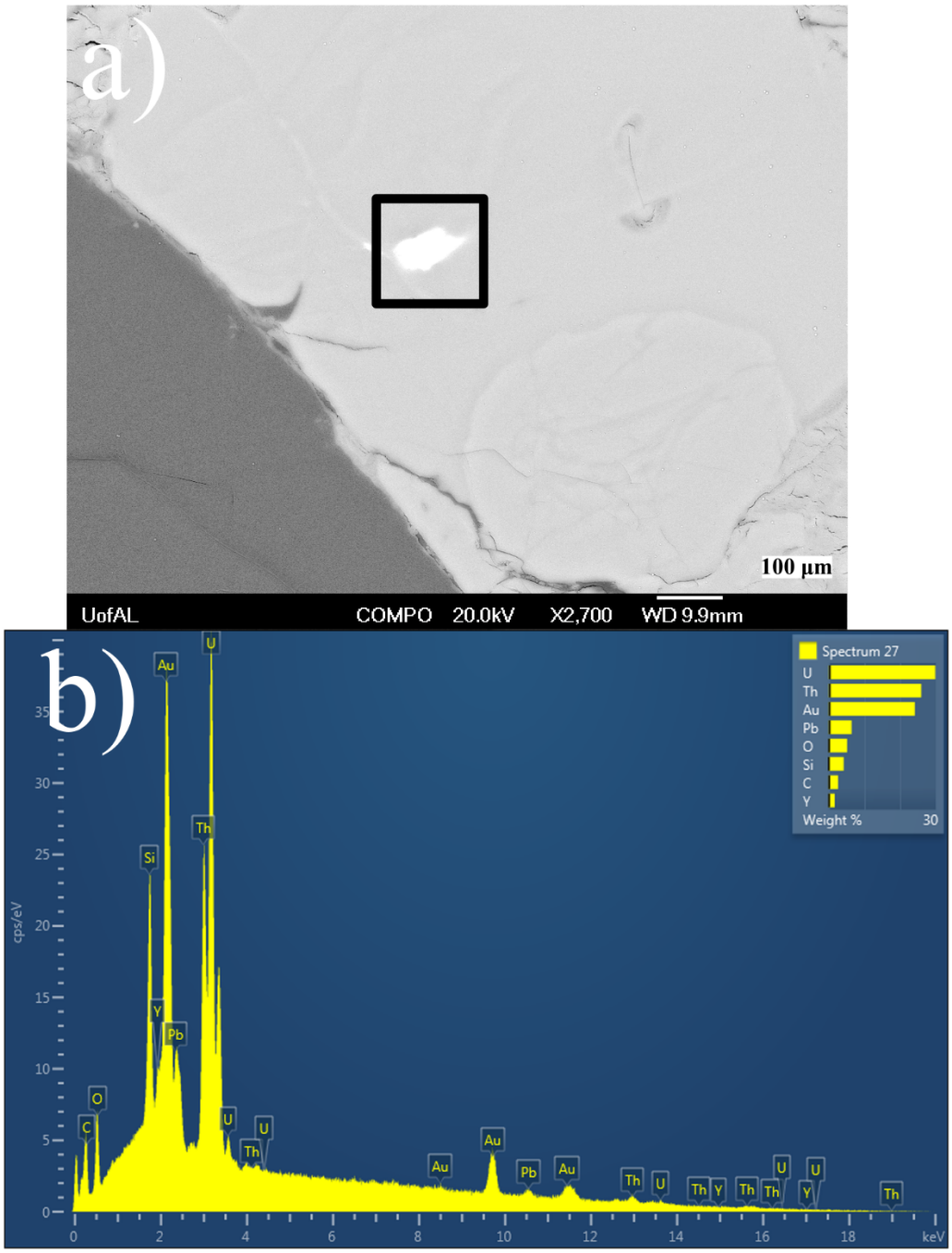


**Figure S8, (a)** BSE image of experimentally shocked zircon and sanidine focusing on a region of backscatter bright material embedded within surrounding ZrSiO4. This image is a close-up view

of the material identified as grain B in the text. **(b)** An EDS spectrum of the backscatter bright region in the box. Peaks indicating the presence of U and Th were identified.

**Figure S9:**

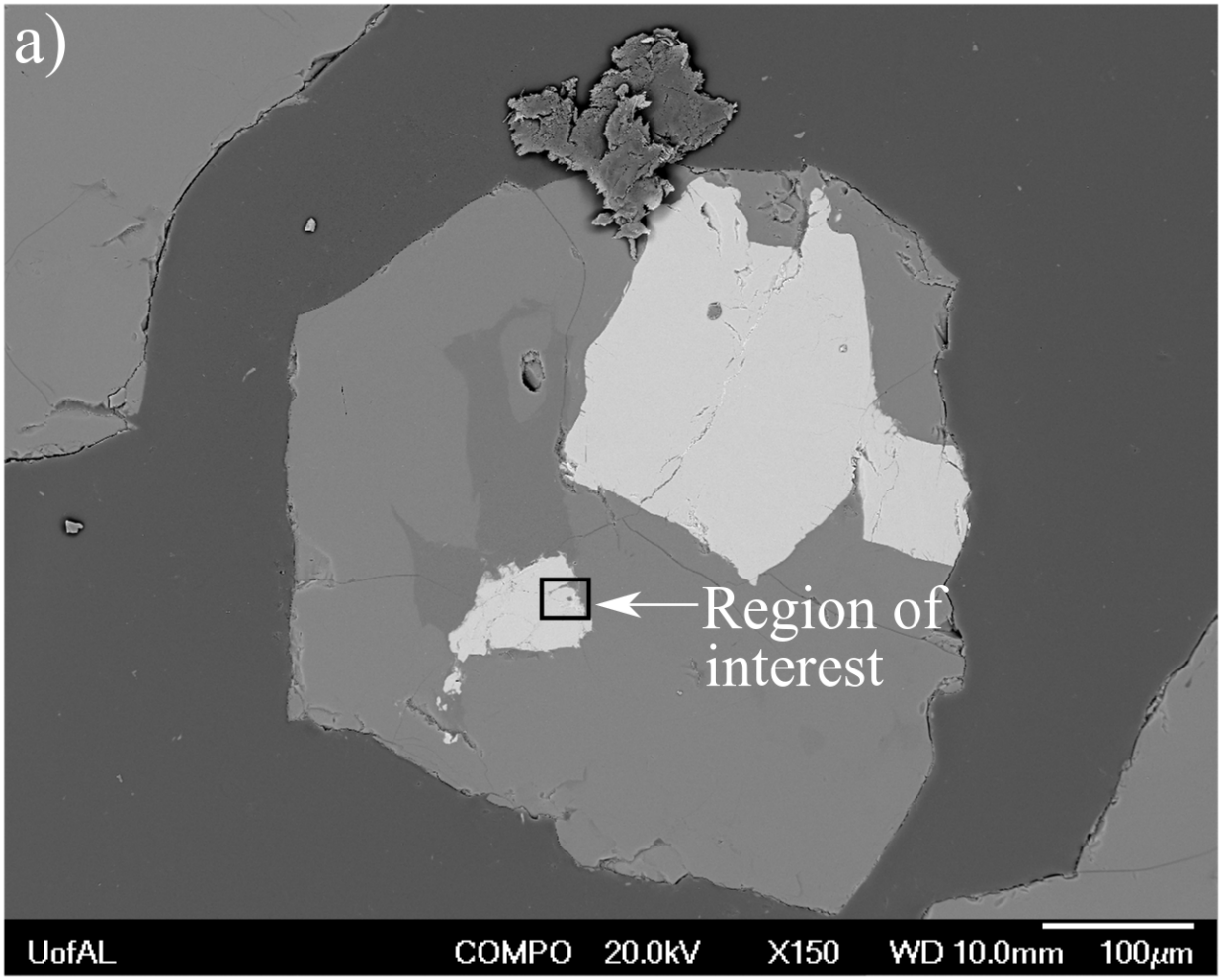


**Figure S9**, shows the context of grain A from **Figure 1a** in the text but with a region of interest to the lower left of grain A identified. More detail on this region in presented in the next supplemental figures (**Figure S10a, S10b, S10c, s10d**).

**Figure S10:**

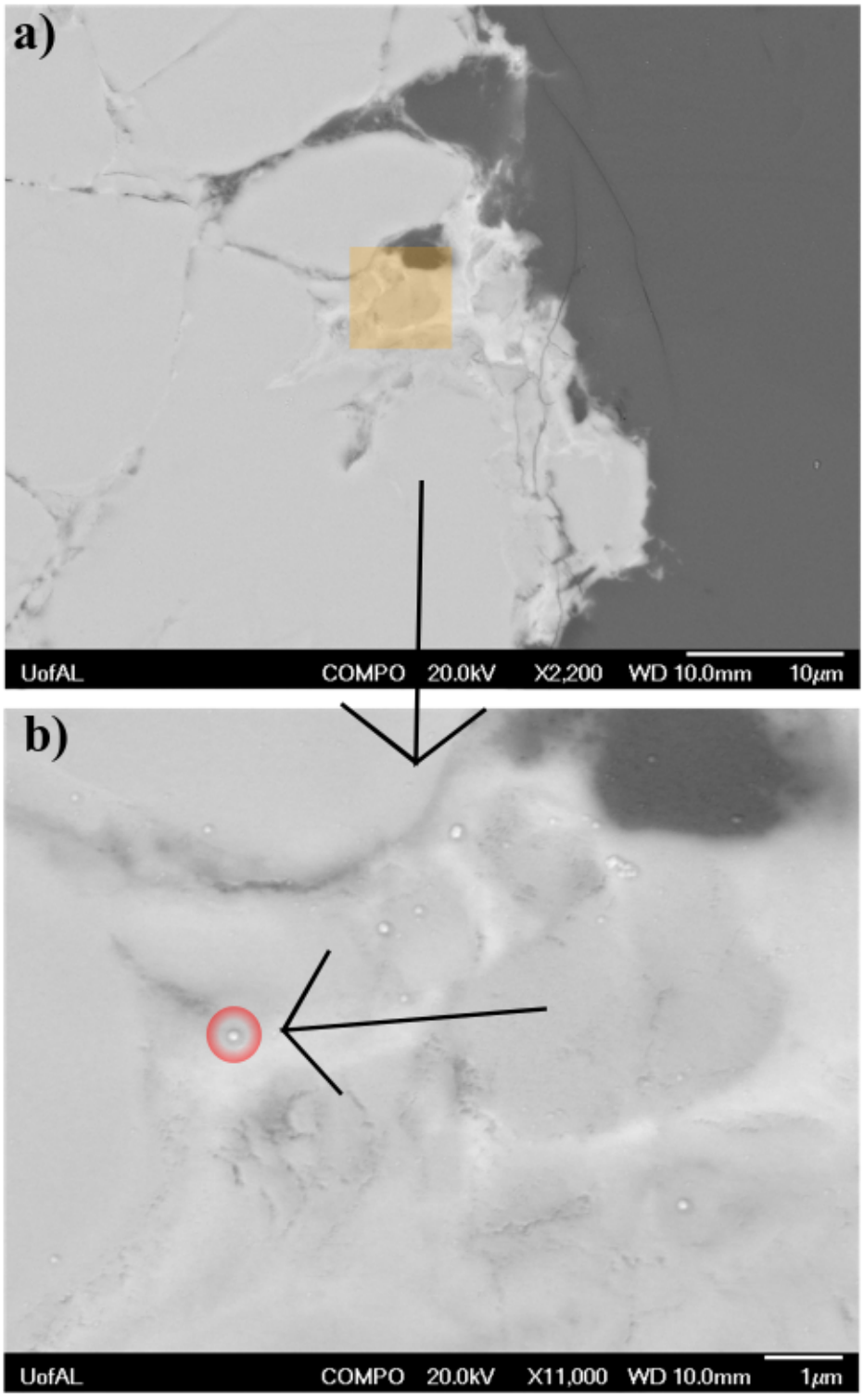
a)
UofAL COMPO 20.0kV X2,200 WD 10.0mm 10μm
b)
UofAL COMPO 20.0kV X11,000 WD 10.0mm 1μm

**Figure S10c:**

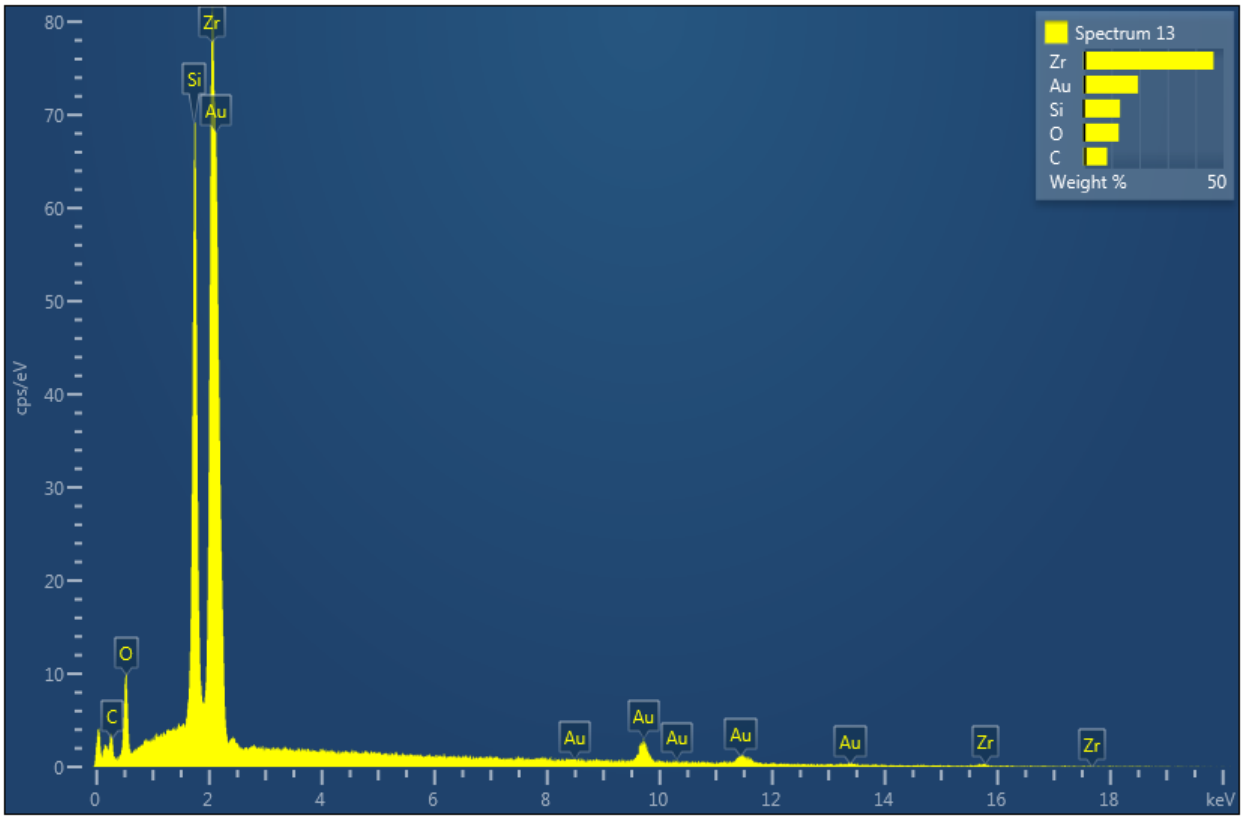
Spectrum 13
Zr
Au
Si
O
C
Weight %
50
cps/eV
keV
Zr
Si
Au
O
C
Au
Au
Au
Au
Au
Zr
Zr

**Figure S10d:**

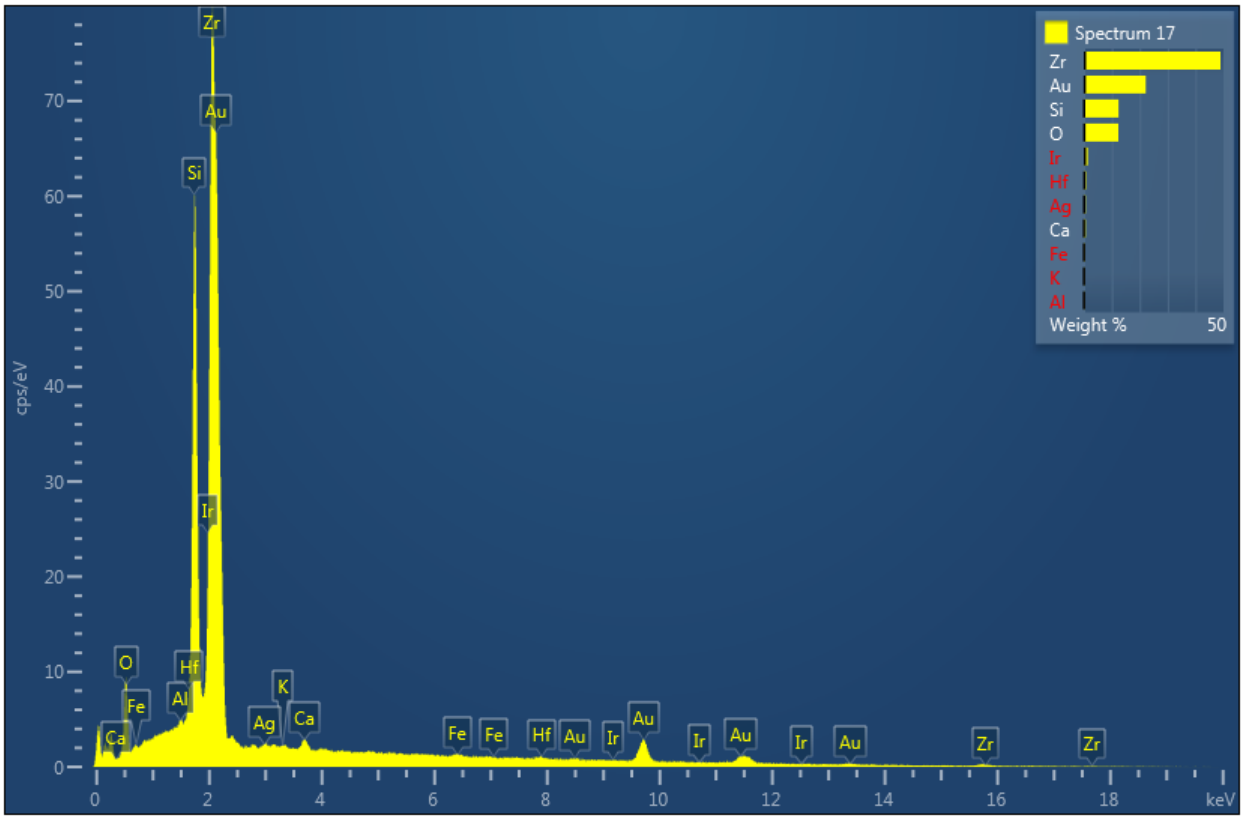


**Figure S10**, (**a)** shows wispy region with **(b)** being a close-up view of this region. **(c)** shows spectra from the grain in **(a)** that is representative of normal zircon, while **(d)** show a spectrum whose interaction volume tried to focus on the bead-like objects in these wispy regions. The spectrum from the bead also appears high in Zr with Zr content being very close to over 50 wt%.

**Figure S11:**

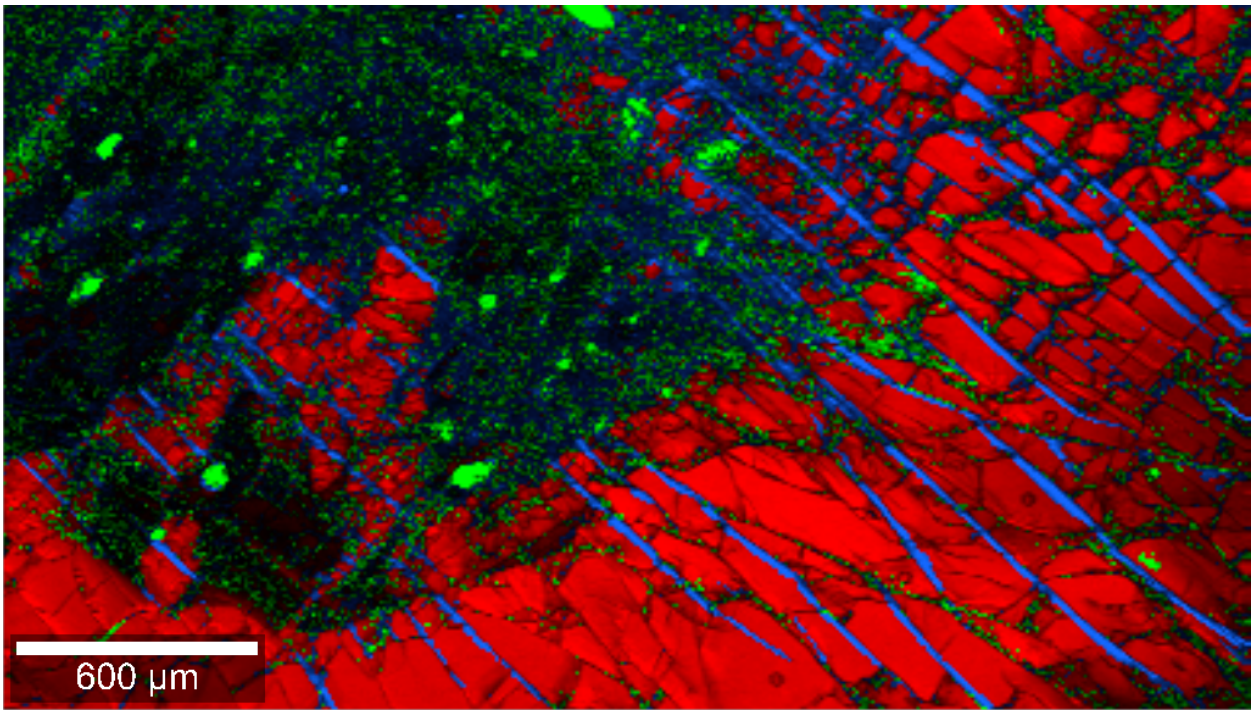


**Figure S11,** This is a re-processing of the Raman spectral map in the text (**Figure 3c**) with red set to identify zircon regions, green for carbonate regions, and blue for possible uranophane.

**Figure S12:**

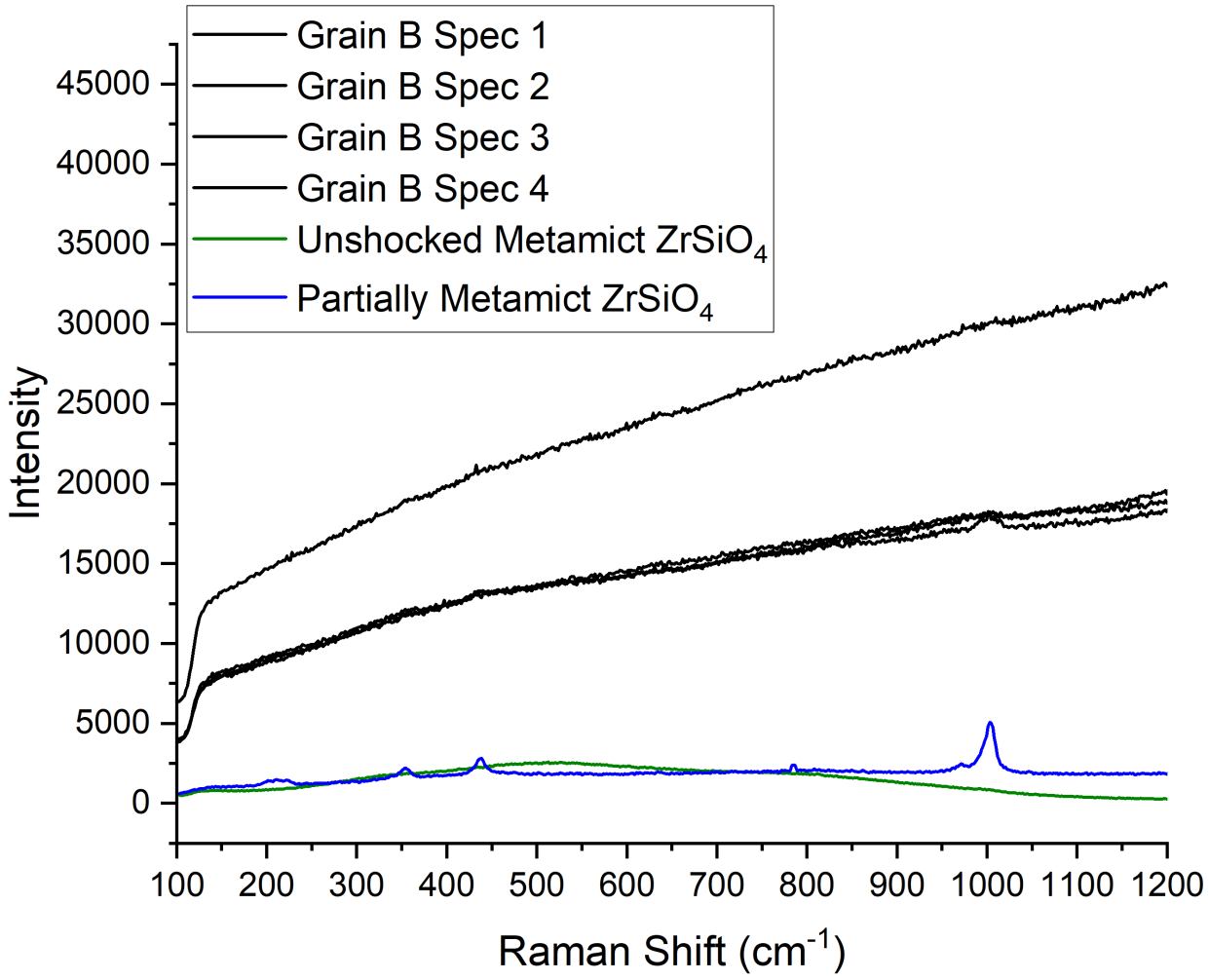


**Figure S12,** Multiple Raman spectral analysis of grain B from the text. Lack of any bands for zircon and reidite as well as a relatively broad flat spectrum indicate this grain has very little structure. It could have been damaged during the shock experiment, or may have already been metamict at the start of the experiment. Spectra from the metamict regions on the starting zircon are presented for comparison.

**Figure S13:**

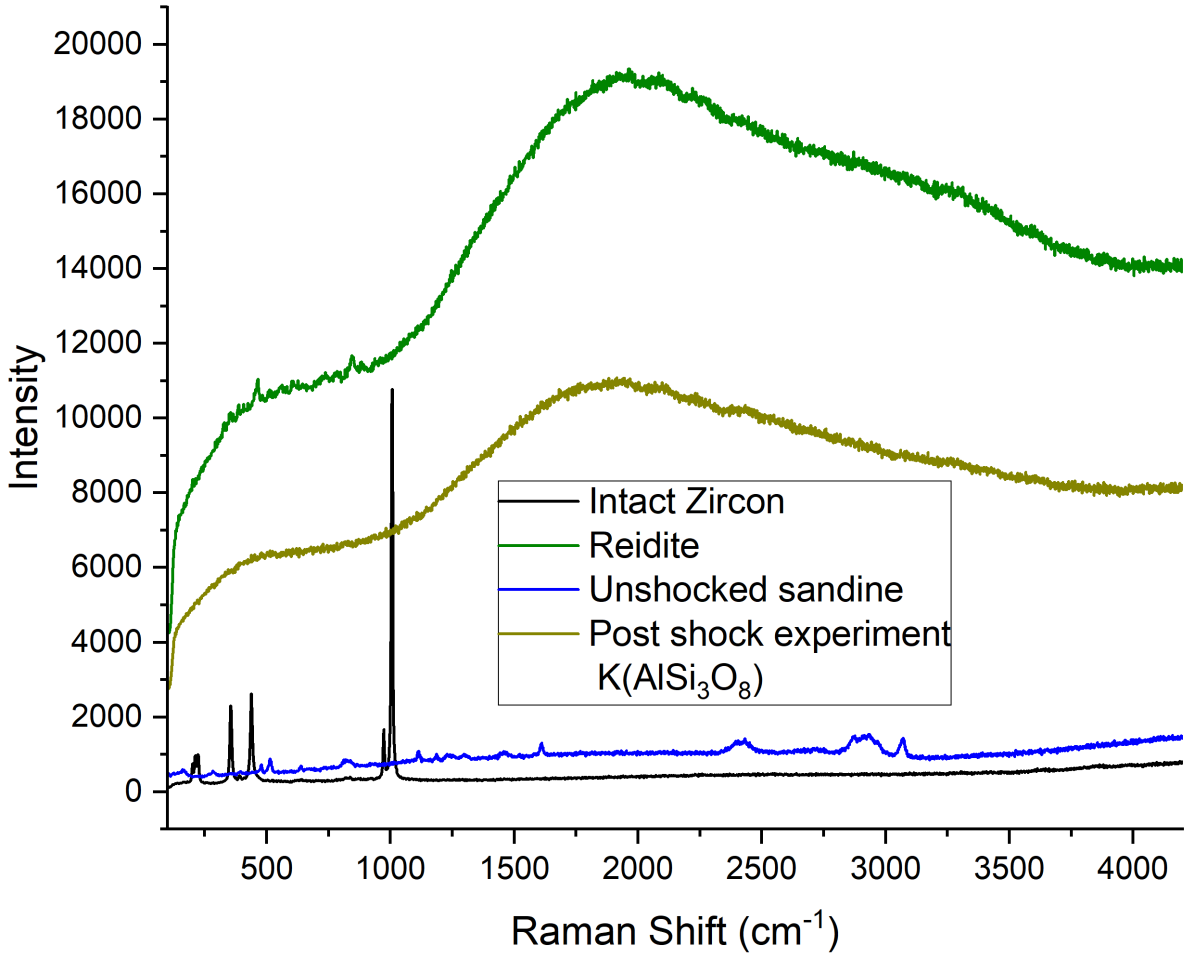


**Figure S13,** The same Raman spectral analyses as presented in Figure 2 in the main text but with the x-axis plotted out to 4200 $cm^{-1}$.

**Figure S14:**

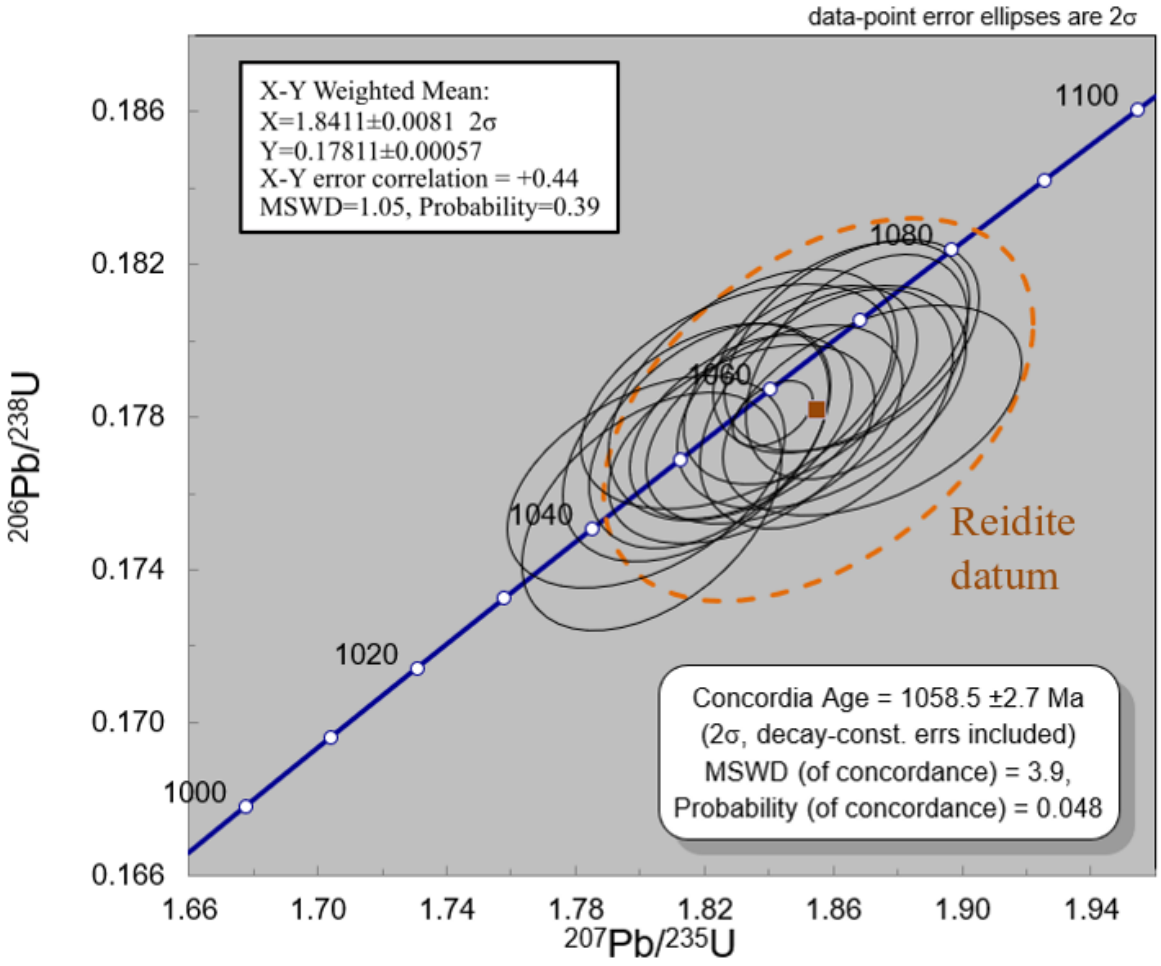


**Figure S14,** U-Pb concordia graph of a vertical traverse on an unshocked portion of the starting zircon grain and a datum from the post-shock experiment reidite based only on the LA-ICP-MS data. The black ellipses mark the error ellipses of measurements taken on the unshocked zircon while the square orange data-point with dashed line mark the sole LA-ICP-MS reidite measurement. The Pb/U measurements for the reidite are directly plotted as a square data-point and dashed error ellipse. This plot was made using the Isoplot software. No obvious difference between the U-Pb isotopic content of reidite and unshocked zircon is seen. This concordia age is

similar to but slightly younger than the LA-ICP-MS $^{207}Pb/^{206}Pb$ age of 91500 zircon which dates to 1065.4 ± 0.3 Ma in Wiedenbeck et al. (1995).

**Figure S15:**

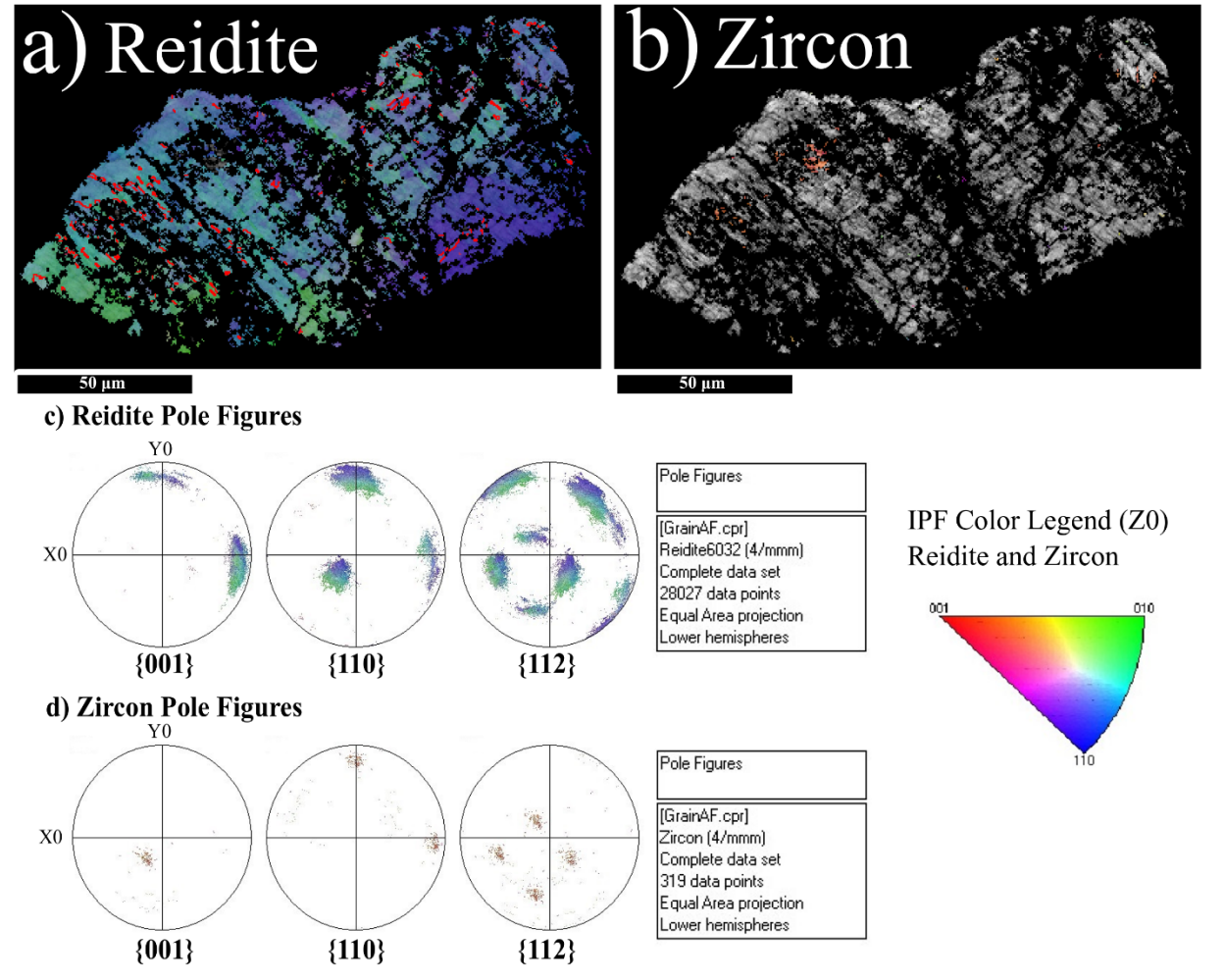


**Figure S15,** More EBSD inverse pole figure color (z direction) maps of another primarily reidite grain. **(a)** shows more {112} twin planes in recovered reidite. **(b)** shows that only a small amount of material indexed as zircon in this grain. Pole figures for **(c)** reidite and **(d)** zircon are shown.

**Figure S16:**

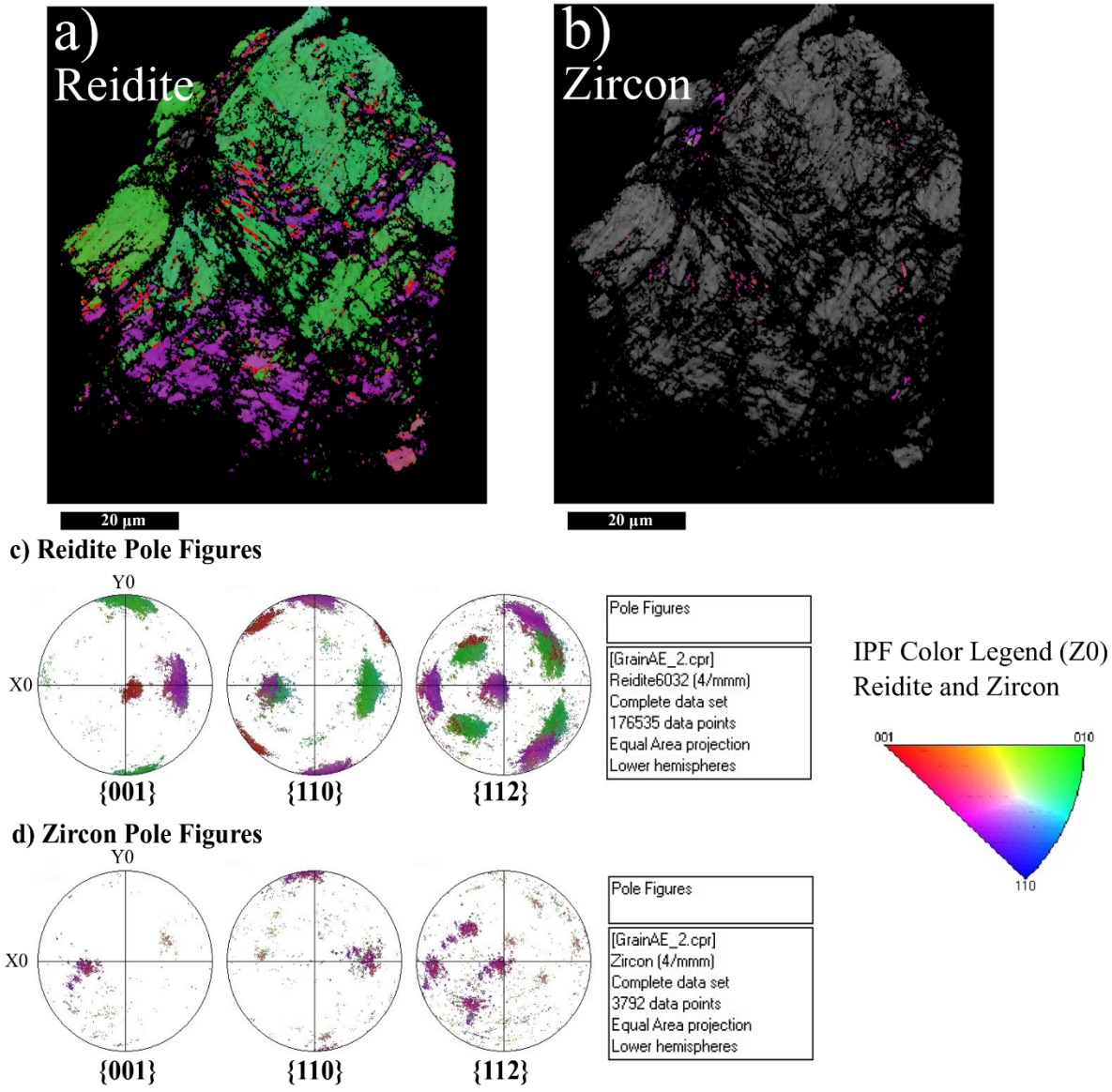


**Figure S16,** Another grain that mostly indexed as **(a)** reidite. **(b)** shows material that indexed as zircon. **(c)** Pole figures for reidite and **(d)** zircon are shown.

**Figure S17:**

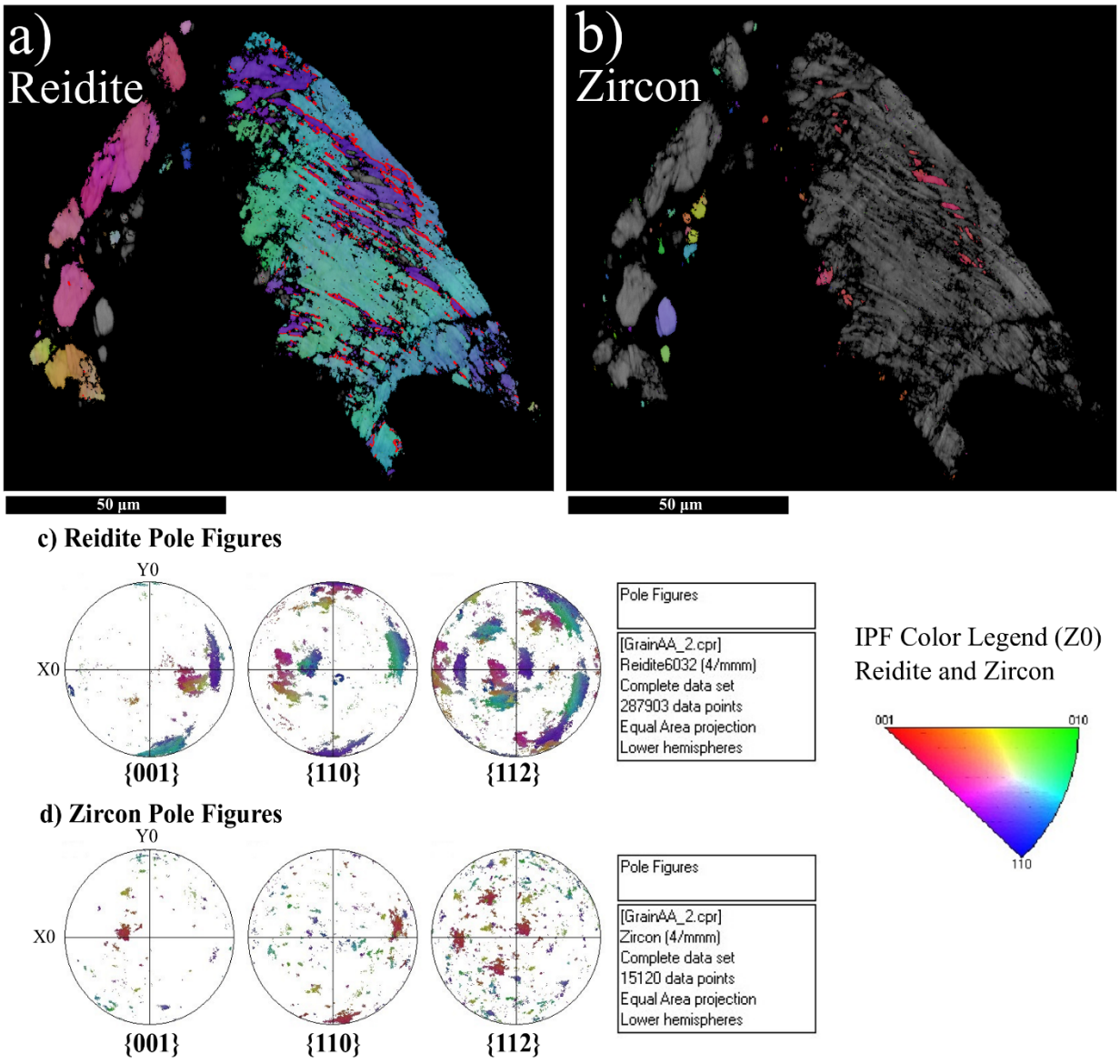


**Figure S17, (a)** More pictured grains that largely identified as reidite. More {112} twinning planes can be seen as the red lines in the right-hand side of **Figure S18a**. **(b)** Material that indexed as zircon. **(c)** Pole figures for this reidite and **(d)** zircon material are shown.

**Figure S18:**

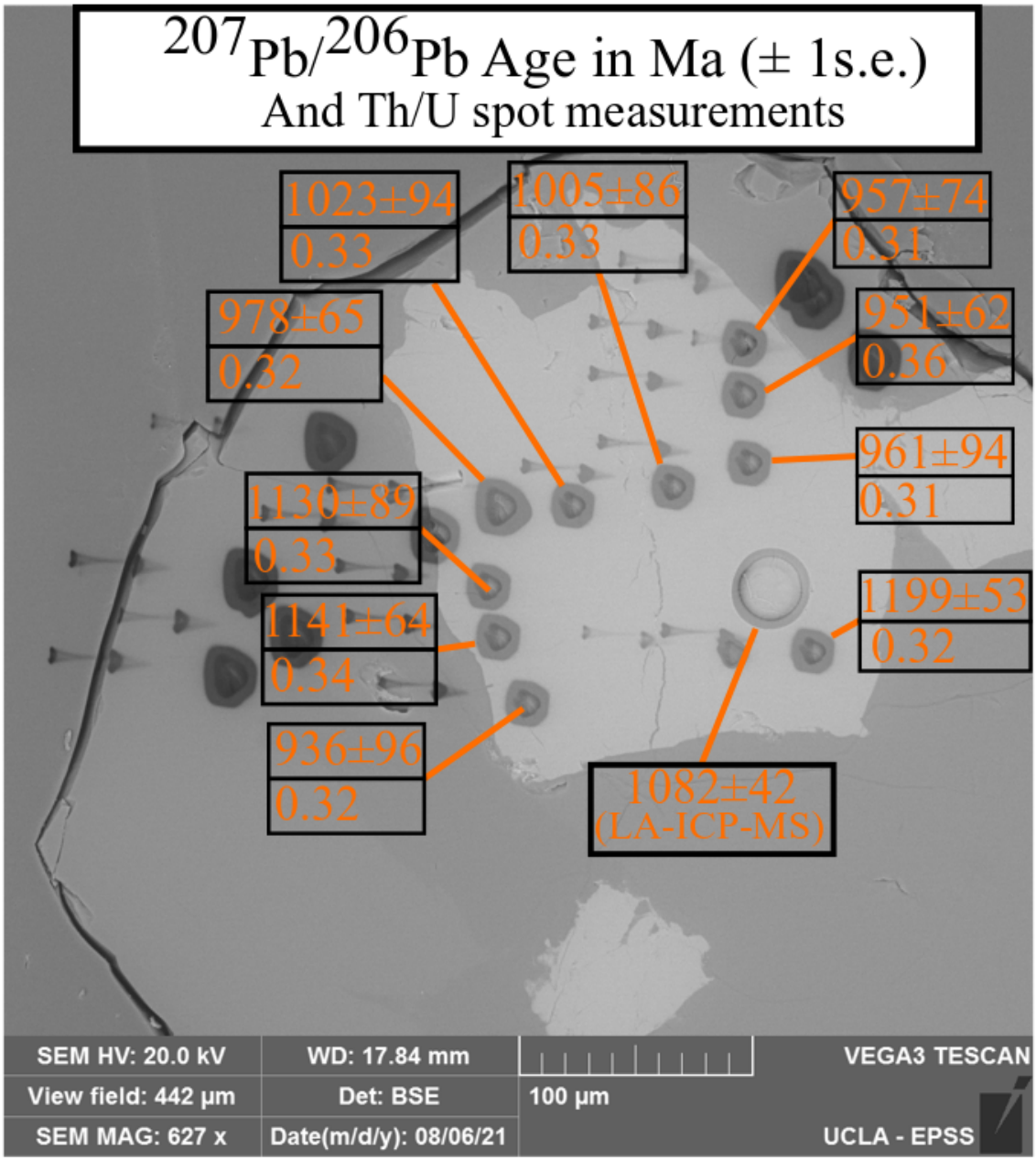


**Figure S18,** An alternative version of **Figure 8** in the text which shows measured Th/U at each of the SIMS spots.

**Figure S19:**

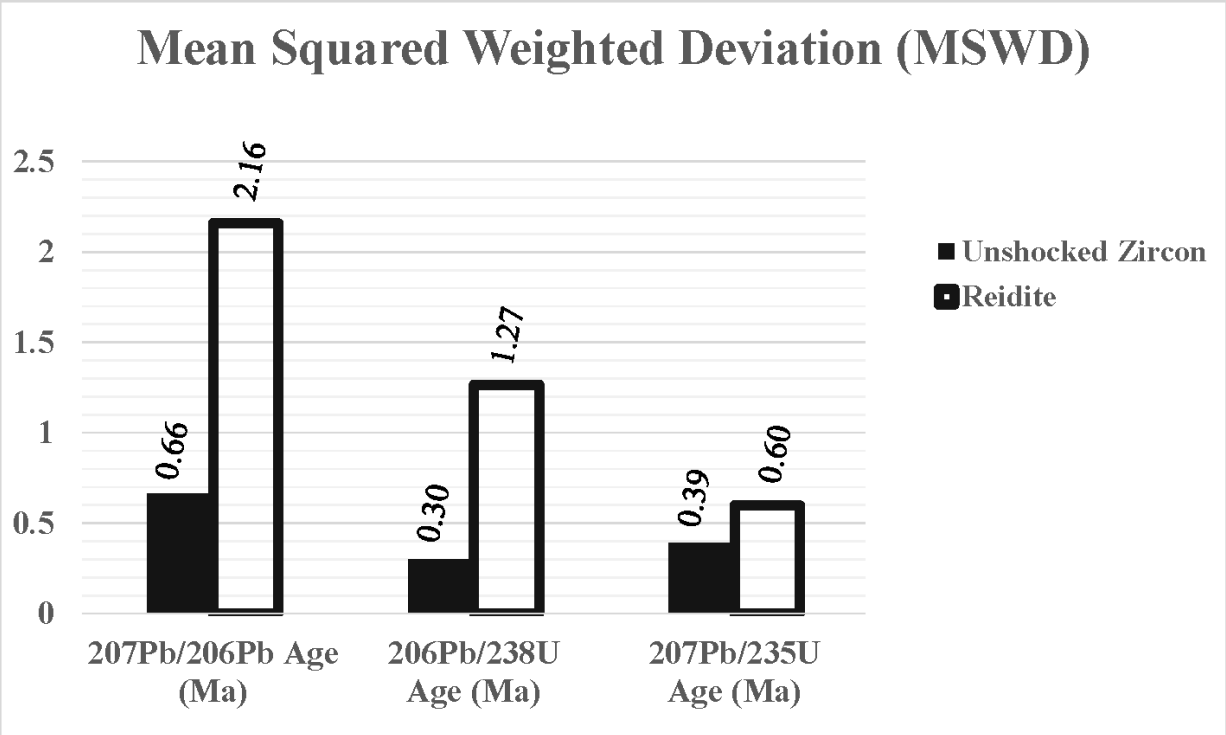


**Figure S19,** A comparison of the MSWD for the U-Pb ages of the unshocked intact zircon and post-shock experiment reidite as analyzed by SIMS.